Naval Research Laboratory

Washington, DC 20375-5320

NRL/FR/5303--12-10,227

Flat-Top Sector Beams Using Only Array Element Phase Weighting: A Metaheuristic Optimization Approach

Irwin D. Olin

Sotera Defense Solutions, Inc.
McLean, Virginia

October 10, 2012

REPORT DOCUMENTATION PAGE

Form Approved
OMB No. 0704-0188

1. REPORT DATE *(DD-MM-YYYY)*	**2. REPORT TYPE**	**3. DATES COVERED** *(From - To)*
10-10-2012	Formal Report	

4. TITLE AND SUBTITLE

Flat-Top Sector Beams Using Only Array Element Phase Weighting:
A Metaheuristic Optimization Approach

5a. CONTRACT NUMBER

5b. GRANT NUMBER

5c. PROGRAM ELEMENT NUMBER

6. AUTHOR(S)

Irwin D. Olin*

5d. PROJECT NUMBER
9741

5e. TASK NUMBER

5f. WORK UNIT NUMBER

7. PERFORMING ORGANIZATION NAME(S) AND ADDRESS(ES)

Naval Research Laboratory
4555 Overlook Avenue, SW
Washington, DC 20375-5320

8. PERFORMING ORGANIZATION REPORT NUMBER

NRL/FR/5303--12-10,227

9. SPONSORING / MONITORING AGENCY NAME(S) AND ADDRESS(ES)

Office of Naval Research
1 Liberty Center
875 North Randolph Street
Code 31, Suite 1425
Arlington, VA 22203-1995

10. SPONSOR / MONITOR'S ACRONYM(S)

ONR

11. SPONSOR / MONITOR'S REPORT NUMBER(S)

12. DISTRIBUTION / AVAILABILITY STATEMENT

Approved for public release; distribution is unlimited.

13. SUPPLEMENTARY NOTES

*Sotera Defense Solutions, Inc., McLean, VA 22102-5011; Naval Research Laboratory retiree.

14. ABSTRACT

The development of wide "flat-top" sector main beams by control of only the excitation phase of phased array elements is described. Pattern parameters are determined by an optimization approach using Visual Basic macros that control the repetitive application of Microsoft Excel's Solver spreadsheet add-in. By only controlling element phases with maximum equal amplitude signals, maximum integrated beam power is achieved. The basic common structure is a linear array of equally spaced elements optimized in a single angular plane. Applied to a square or triangular grid array, their parameters are combined to produce beams along two orthogonal principal planes, resulting in a square or rectangular flat-top profile. Circularly symmetric beam profiles are developed using a circular grid array. The impact of optimization, element phase precision, sector ripple, sidelobe levels, and integrated power are analyzed in some detail. The goal is to provide sufficient documented procedural detail that can then be specialized to specific array requirements.

15. SUBJECT TERMS

Phase-only beam steering
Optimization
Phased array
Excel

16. SECURITY CLASSIFICATION OF:			**17. LIMITATION OF ABSTRACT**	**18. NUMBER OF PAGES**	**19a. NAME OF RESPONSIBLE PERSON**
a. REPORT	**b. ABSTRACT**	**c. THIS PAGE**			James Alter
Unclassified	Unclassified	Unclassified	Unlimited	53	**19b. TELEPHONE NUMBER** *(include area code)* 202-767-3517

Standard Form 298 (Rev. 8-98)
Prescribed by ANSI Std. Z39.18

This page
intentionally
left blank

CONTENTS

This page
intentionally
left blank

FLAT-TOP SECTOR BEAMS USING ONLY ARRAY ELEMENT PHASE WEIGHTING: A METAHEURISTIC OPTIMIZATION APPROACH

SUMMARY

The development of wide "flat-top" sector main beams by control of only the excitation phase of phased array elements is described. Pattern parameters are determined by an optimization approach using Visual Basic (VB) macros that control the repetitive application of Microsoft Excel's "Solver" spreadsheet add-in. By only controlling element phases with maximum equal amplitude signals, maximum integrated beam power is achieved. The basic common structure is a linear array of equally spaced elements optimized in a single angular plane. Applied to a square or triangular grid array, their parameters are combined to produce beams along two orthogonal principal planes, resulting in a square or rectangular flat-top profile. Circularly symmetric beam profiles are developed using a circular grid array. The impact of optimization, element phase precision, sector ripple, sidelobe levels, and integrated power are analyzed in some detail. The goal is to provide sufficient documented procedural detail that can then be specialized to specific array requirements.

BASIC CONSIDERATIONS

The far-field beam pattern of an array of elements is a function of the characteristics of the individual elements, their spacing within the array, and the element excitation amplitudes and phases. With large numbers of elements spaced close enough to avoid the redundant pattern character of grating lobes, the numbers of possible shaped beams are almost limitless. But of particular interest in this work are the aptly named flat-top beams, the general character of which is illustrated in Fig. 1. The shape is characterized by a prescribed main-beam sector region with little ripple, shown in blue, a small angular transition region, shown in grey, and a low-amplitude sidelobe region, shown in red. If each element in the array is assumed radiating nearly isotropic, the fields from each element combine at every angle. The final pattern then results by combining the complex (amplitude and phase) excitation of each of the elements.

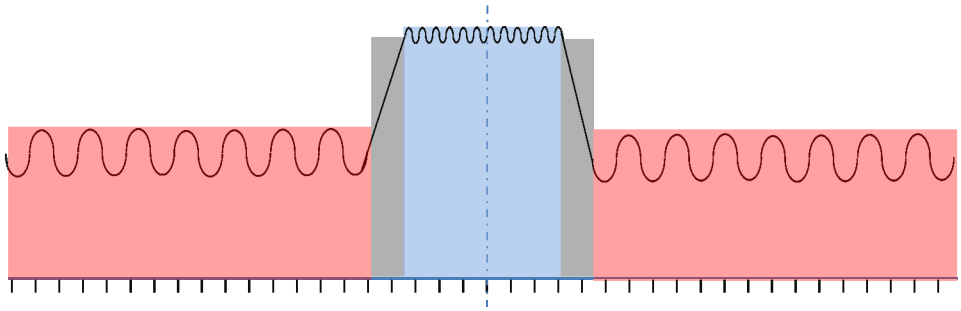

Fig. 1 — Angular sectors of the flat-top beam. A constrained-ripple flat-top is shown in blue, a transition region is shown in gray, and a sidelobe region in red.

Manuscript approved June 30, 2012.

Techniques for shaping these patterns, mostly based on inverse Fourier transforms, are well known and are extensively used. But their fit to a prescribed pattern profile very much depends on *both* the excitation amplitudes and their phases. Removing the amplitude variability is seen as a means to transmit the most power, or receive with the highest gain using an array, but this introduces severe constraints on the design process. On transmission, pattern control is then characterized by manipulating only the phases of each element drive signal.

Consider the simple linear array of isotropic radiating elements depicted in Fig. 2. The line of sight (LOS) at angle θ, projected at the array center, is the normal to a far-range direction in which the composite fields from each of the elements must be added to determine the amplitude at just that angle.

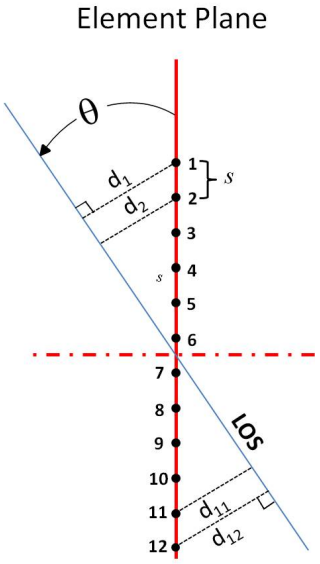

Fig. 2 — Linear array of equally spaced elements with a representative line of sight (LOS) projected on the coordinate origin

The distance to the line from each element point, d_n, then determines the equivalent electrical phase $\beta d_n = 2\pi/\lambda \cdot d_n$. Clearly d_n is a function of the element's location in the array, so that the element spacing, *s*, must be included. This is conveniently expressed in terms of the operating wavelength: $s = \lambda/k$. Typically, $k = 2$, or as part of an equilateral triangular lattice, $k = \sqrt{3}$. Then for the general case of *N*, an even number of elements, the corresponding phase for each element, *n*, is given by

$$\frac{\pi}{k}(N+1-2n)\sin\theta\text{, with } n \le N/2,$$

since the distances are symmetric relative to the array center. Assuming the beam is shaped symmetrically about the coordinate origin, *N*/2 additional phases (δ_n) are added to all *N* array elements. Considering the

geometry and the additional excitation phase, adding δ_n to each of the elements leads to the following equation for the sum of all the components, in which N elements spaced λ/k apart are considered:

$$E(\theta) = 2\sum_{n=1}^{N/2} \varepsilon^{i\delta_n} \cos\left[\frac{\pi}{k}(N+1-2n)\sin\theta\right].$$

Each of the phases can be within an interval $-\pi \le \delta_n \le +\pi$ radians, so even with the 12 elements illustrated in Fig. 2, the number of possibilities is essentially countless, and that is where the solution in this report begins. Except for an additional overall $\sqrt{\cos\theta}$ amplitude factor that modifies the omni-directional character of each element, the preceding equation fully expresses the far-field interactions. An objective then is to find the set of element phases that minimize the sidelobes while constraining the main-beam ripple to a specific value. Adding a further constraint that the phases are within ±2π, this provides a tractable problem for solution. But that too is difficult owing to the periodic nature of the term $\exp(j\delta_n)$. There will be very many optimized minimum or maximum values, so which one is the best? Technically this is a non-convex optimization problem and the answer sought is the global minimum or maximum. The short answer to the approach taken is that the end result may not represent a global minimum. There is the likely possibility that another set, even though providing sidelobes only a very small fractional decibel better, can be found. But the result can be demonstrably close enough, and that is sought here. Moreover, the practical granularity in the phase settings means that even finding the theoretical global minimum set of phases, they will likely not be used in practice.

OPTIMIZATION

Contemporary optimization alternatives such as genetic algorithms [1–9], simulated annealing [10], particle swarm optimization [11], and just random search [12] are all procedures that do not solve the complex electromagnetic array problem. (Of these, genetic algorithms currently appear the most favored, although using them can involve longer optimization time.) One succinctly phrased comment notes that although one may not know how to actually solve a problem, at least a satisfactory answer is recognizable. Rather than solve the problem, the defining equations of these optimization techniques fulfill objectives and constraints that represent a process from which an acceptable result, *independent* of the underlying theory, is generated. Of course this does not imply that the results of these techniques are consistent one with another in detail, as is later illustrated. Basically it all comes down to time, or equivalently, the number of iterations before converging to an acceptable result.

Yet another alternative used in this report repetitively calls the Solver add-in function in an Excel spreadsheet by a Visual Basic macro. Applied to the array problem, Solver uses a classic gradient search technique in which a continuously changing objective of trial values programmed for the minimum sidelobe level in the n-dimensional space is gradually approached by the n-dimensioned vector set of variables. These may be the phases or the several phase-related weights, next described. Finally, macro repetition enables convergence to an *acceptable* solution. For a linear array with a symmetric beam, only $N/2$ element phases are needed. But for a representative 50-element array, this only helps the bookkeeping, since even 25 may be too many to easily handle.

Applied to this specific problem, an especial difficulty is the initial set of element phases. The optimization process uses the initial set as a base for ensuing trials to reach an objective fit, along with any included constraints. So, common to all solutions using optimization, the issue of where to start must be confronted. Without a reasonably good initial set, the result is often that no feasible solution exists,

even though the equations describing the pattern are correct. A premium Solver version by Frontline, the developer of the Excel add-in, provides a multistart option with optimization proceeding with five different starting sets (of their choice) following a determination of the best to define the closest to a global optimum, but it too is often poorer than one using a better starting set.

INITIAL VALUES

The initial set selection need not be an exhaustive or a blind process. The familiar "sinX/X" pattern results in using the combined fields from a uniformly phase-weighted array of elements. For a symmetric linear array of N elements spaced λ/k apart, as cited on p. 3, the resulting equation is

$$E(\theta) = 2\sum_{n=1}^{N/2} \cos\left[\frac{\pi}{k}(N+1-2n)\sin\theta\right].$$

For sector beamwidths little different from that defined by this pattern, Solver defines the initial phase set that can then be incrementally changed to accommodate ever-widened beams. If the increments are small, the likelihood of missing an acceptable "optimum" solution is low. Subsequent incremental widening can be continued until the required beam parameters are met. But for wide beamwidths this may not be as useful as a comparatively simple alternative. In a 2004 paper, Marcaccioli, Gatti, and Sorrentino [13] proposed phase-only synthesis for a linear array that defined the element phases in terms of just a few Chebyschev polynomial weights, of the first kind. The pattern fit is determined by the element phases using only the weights of several even-ordered polynomials which are just expansions of these phases. Recall that these polynomials can be expressed as: $T_0(x) = 1$, $T_1(x) = x$, with the recurring relationship, $T_{n+1}(x) = 2xT_n(x) - T_{n-1}(x)$. Alternatively, using the normalized distance of each element from the array center, defined by $k(n) = -1 + 2\frac{n-1}{N-1}, n = 1,2,,,N$, the corresponding polynomials are defined by

$$T_2(k) = 2k^2 - 1, \;\; T_m(k) = \cos\left(m\cos^{-1}k\right).$$

The set of phase weights is then defined by the polynomials and their weights, W_m. Assuming six even-ordered polynomials are used, the phase weights are

$$\delta_n = W_2T_2k(n) + W_4T_4k(n) + W_6T_6k(n) + ... + W_{12}T_{12}k(n).$$

As a result, the number of degrees of freedom is drastically reduced; in fact the numbers of elements are not directly involved. The approach even appears independent of the number of elements in the array. But since it is the derived phases, rather than the weights, that control solution acceptance, this method can be used regardless of the numbers of elements. An additional advantage is gained by only using even-ordered polynomials, since these polynomials show the even-ordered response familiar in circuit design and are well matched to a symmetric array of elements. But, as described in the section "Different

Starting Sets: Acceptable Results," the relationship between the element phases derived from Chebyschev polynomials is an approximation, albeit convenient in terms of computation efficiency.

That is then both the advantage and disadvantage of this approach. There are fewer degrees of freedom to use, but also there are fewer degrees of freedom to match an objective pattern. The precision or resolution of the weights is increasingly important in fulfilling the optimization criteria. But it has been found to provide a much better starting weight set, from which a VB macro using a "do-loop" program can continuously refine the set to an acceptable result. Of course, even this also requires an initial set. But among the specific weights it has been found that the value of W_2 (near end value, rather than center) far exceeds and essentially defines the flat-top width. For a half-width flat-top of $\Delta\theta$ (degrees), a good empirical starting value is $W_2 = \Delta\theta/3$, with the remaining weights each set equal to unity. Since the weights define element phases, it is the phases that measure the fit to the optimization objective, along with any defined constraints. Optimization is essentially a process that is blind to the underlying electromagnetic field relationship depicted by the defining equation, so the phases defined by a good weight set can then also be further optimized, if required.

OPTIMIZATION CONVERGENCE

As described in this report, the optimization technique is a metaheuristic process, iteratively comparing the current and prior results as illustrated in Fig. 3 by iterations of the Solver function under VB control. Three columns of parameters, either the Chebyschev polynomial weights or the element phases, are varied and circulated during the optimization decisions. For a specified flat-top width and transition width, just one decision is involved, the maximum pattern sidelobe, with a defined and constrained main-beam ripple. (Additional constraints confining the element phases within ±π radians may be further included when optimizing the phases directly.) The blue column contains the best set of weights or phases during the iterations. The values in the green set contain a small random change in each of the blue values. Using the Excel RAND() function, this change is made with each loop iteration. The red set of phase values is the current set used to calculate the array pattern during each optimization. The VB macro changes these values as the equivalent multidimensioned vector of the set is directed to a trial-optimized result. During each of the iterations, some trial results cannot be met, but eventually one is found and the set retained without change. (Note that even a single iteration may involve a large number of trial values; several hundred are not unreasonable). If the result is better than found before, it is copied to the blue set.

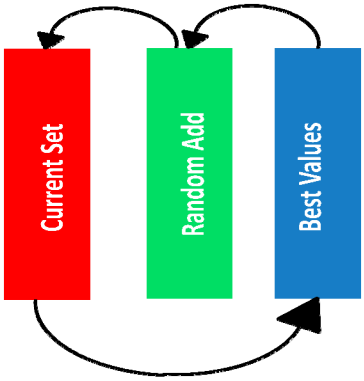

Fig. 3 — Lists of all element weights circulating in the Visual Basic macro loop

If it is not, then the green set, which is changed, is copied to red and the optimization loop continued. The idea is to continue to work only with small randomized changes to the best available set. These changes move the next trial result away from the prior result, so a new, possibly better, result will be found. A copy of the VB macro used for optimizing initial phase lists that includes the spreadsheet references is included in Appendix B. The macro for the Chebyschev weight optimization is similar, with the addition of a spreadsheet that defines the phase list from the list of optimized Chebyschev polynomial weights.

REPRESENTATIVE ROW ARRAY RESULTS

Although the overall objective of the work described here is the design of two-dimensional arrays with specific scanned patterns, the basic structures that are repetitively used are simple one-dimensional arrays of equally spaced elements. Regardless of the pattern requirements, the associated element phase values are derived solely from these simple arrays.

Assuming a linear array of 50 elements spaced λ/2 apart, parameters for non-scanned flat-top sector beams with widths of ±5°, ±10°, ±20°, ±30°, ±40°, and ±50° were each first developed using just the Chebyschev weights. The associated optimizations used just the 10 weights, but changes during each of the optimization iterations were determined by their impact on the pattern, which was *solely* a function of the element phases. Then the resulting independent 25 phases from each of these were further optimized for minimum ripple. The effect of element pattern on each flat-top was represented by a multiplicative factor of $\sqrt{\cos\theta}$ applied to each of the array E-field values. Copies of the optimized Chebyschev weight set and the phase shaping pattern set following further optimization are in Appendix A. The results are shown in Figs. 4 through 9; each was assumed satisfactory when many repeated optimizations produced little change in the quality of the pattern. Again, this does not confirm that any are globally optimum. But global relevance should not be preeminent; the result should be framed in terms of its fulfilling the concept objective. As my former supervisor once remarked, is the "best of good enough" sufficient?

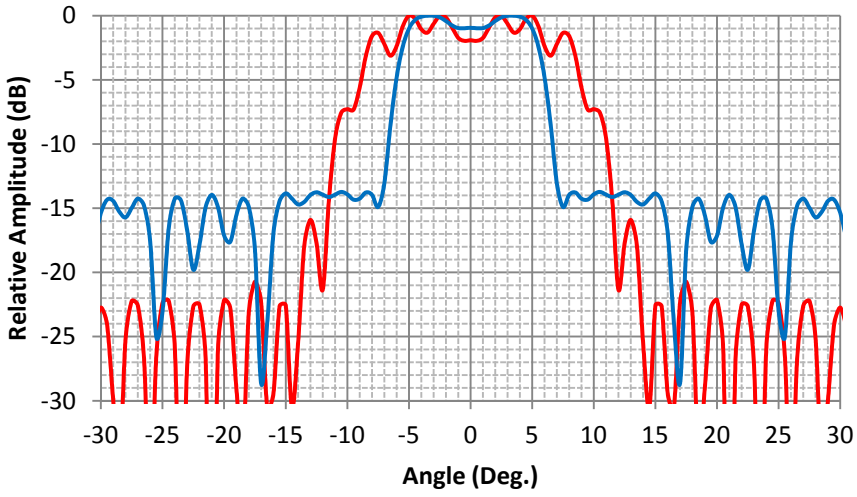

Fig. 4 — Angular array patterns for a symmetric linear array of 50 elements spaced λ/2 apart using phase-only weighting. Both plots were optimized for a ±5° main beam. Results optimizing just 10 even-ordered Chebyschev weights are shown in red, while a further optimization of the derived element phases is shown in blue.

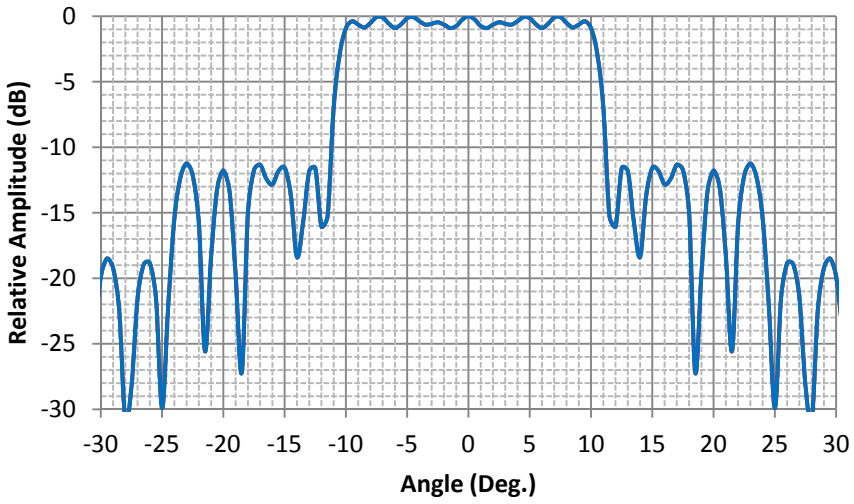

Fig. 5 — Angular array pattern for a symmetric linear array of 50 elements spaced λ/2 apart using phase-only weighting optimized for a ±10° main beam. The results using just the 10 even-ordered Chebyschev weights were satisfactory. Little improvement resulted by further optimization of the corresponding element phases within a ±90° interval.

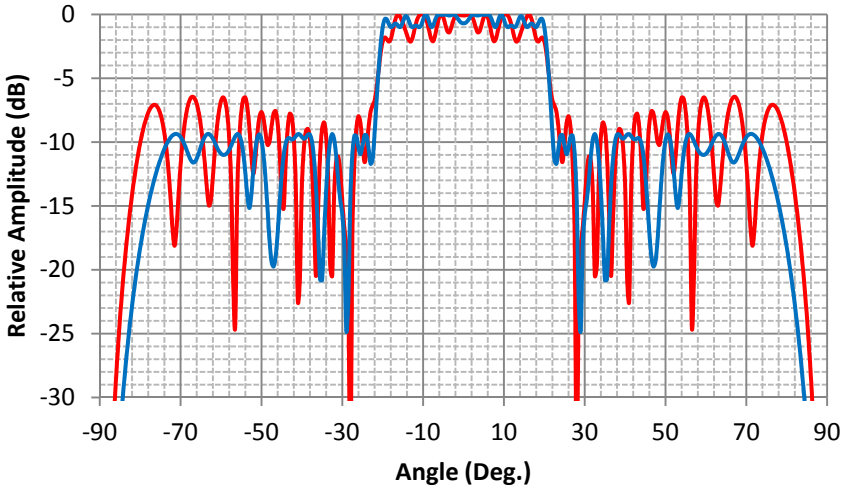

Fig. 6 — Angular array patterns for a symmetric linear array of 50 elements spaced λ/2 apart using phase-only weighting. Both plots were optimized for a ±20° main beam. Results optimizing just 10 even-ordered Chebyschev weights are shown in red, while a further optimization of the derived element phases is shown in blue.

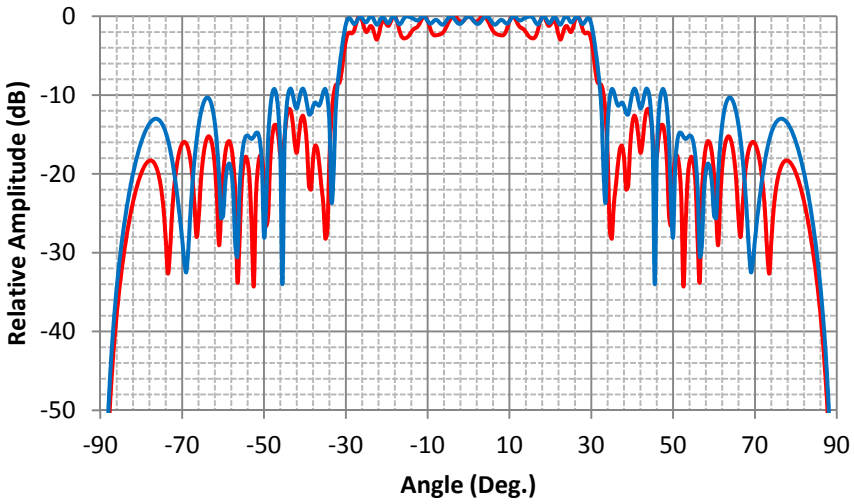

Fig. 7 — Angular array patterns for a symmetric linear array of 50 elements spaced λ/2 apart using phase-only weighting. Both plots were optimized for a ±30° main beam. Results optimizing just 10 even-ordered Chebyschev weights are shown in red, while a further optimization of the derived element phases is shown in blue.

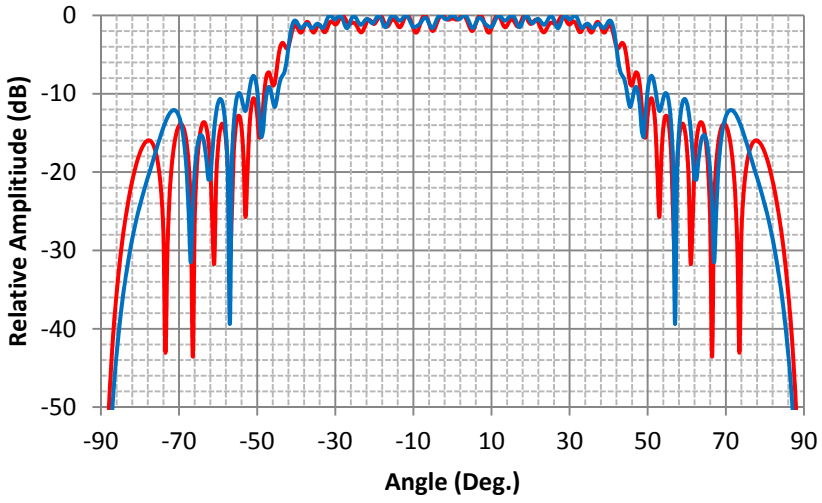

Fig. 8 — Angular array patterns for a symmetric linear array of 50 elements spaced λ/2 apart using phase-only weighting. Both plots were optimized for a ±40° main beam. Results optimizing just 10 even-ordered Chebyschev weights are shown in red, while a further optimization of the derived element phases is shown in blue.

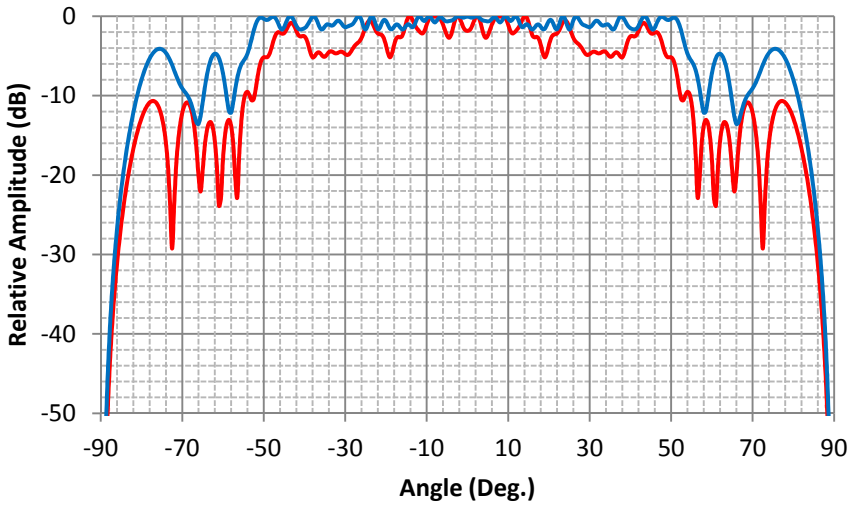

Fig. 9 — Angular array patterns for a symmetric linear array of 50 elements spaced λ/2 apart using phase-only weighting. Both plots were optimized for a ±50° main beam. Results optimizing just 10 even-ordered Chebyschev weights are shown in red, while a further optimization of the derived element phases is shown in blue.

The variability of the results using optimization is evident by comparing these results. For the patterns using just the 10 Chebyschev weights, only a few hundred successive optimizations were necessary until very little improved performance was apparent. These results are illustrated in the curves plotted in red. However, the 10 degrees of freedom used was double that originally used by the authors in Ref. 13. No further attempt was made to explore further increases in the numbers of these weights. In general it was found that lower beam ripple is accompanied by higher maximum sidelobes.

DIFFERENT STARTING SETS; ACCEPTABLE RESULTS

The independence, even irrelevance, between the details of the array electromagnetic theory and an acceptable solution using any of the optimization methods was noted above. It is also well known that the results using optimization are very dependent on the initial parameters. In this report these parameters are the initial set of element shape phases which are used in repetitive optimization. Then, since the goal is a "satisfactory" rather than a "global optimum" set of weights, otherwise disparate initial sets of these parameters may each result in acceptable patterns. An example is shown in Fig. 10(a) in which a set of 25 phases for a symmetric linear array of 50 elements equally spaced by $\lambda/\sqrt{3}$ was required. The objective was a ±10° flat-top, ripple equal or less than ±0.5 dB, and maximum sidelobes of −10 dB. The initial weight sets differed, and the two independent optimized results, shown in blue and red, appeared very different, but since each fulfilled the objective and constraints, both are acceptable. Each set required about 200 repetitions; further repetitions differed very little. Clearly, neither phase set can be identified as a global optimum, but the difference is an important aspect of the optimization process, regardless of method used. The optimized set shown in red is typical of those detailed in Appendix A. The phase of the elements at each end is higher than those near the center (element 25) of the array. The corresponding array pattern is shown in red in Fig. 10(b). The second optimized phase set, shown in blue in Fig. 10(a), varies differently, low at each end and higher in the center. But the corresponding array pattern, in blue in Fig. 10(b), confirms that both sets are acceptable, although the source sets appear very different. However, there is a demonstrable relationship as shown in the other two phase sets in Fig. 10(a). First, plotting the supplement of the phase angles in blue, shown dashed in the figure, reveals the similarity with

the red set. Then the angles in that set can be translated by adding a constant value to each angle to produce the close match shown in green. Simply adding or subtracting a fixed value to each phase has no effect on the result. Equivalently it is just a translation of the LOS that is unrelated to the patterns. Overall there is a close similarity, but not an exact equivalence between the two phase sets, since neither set likely corresponds to the "global optimum."

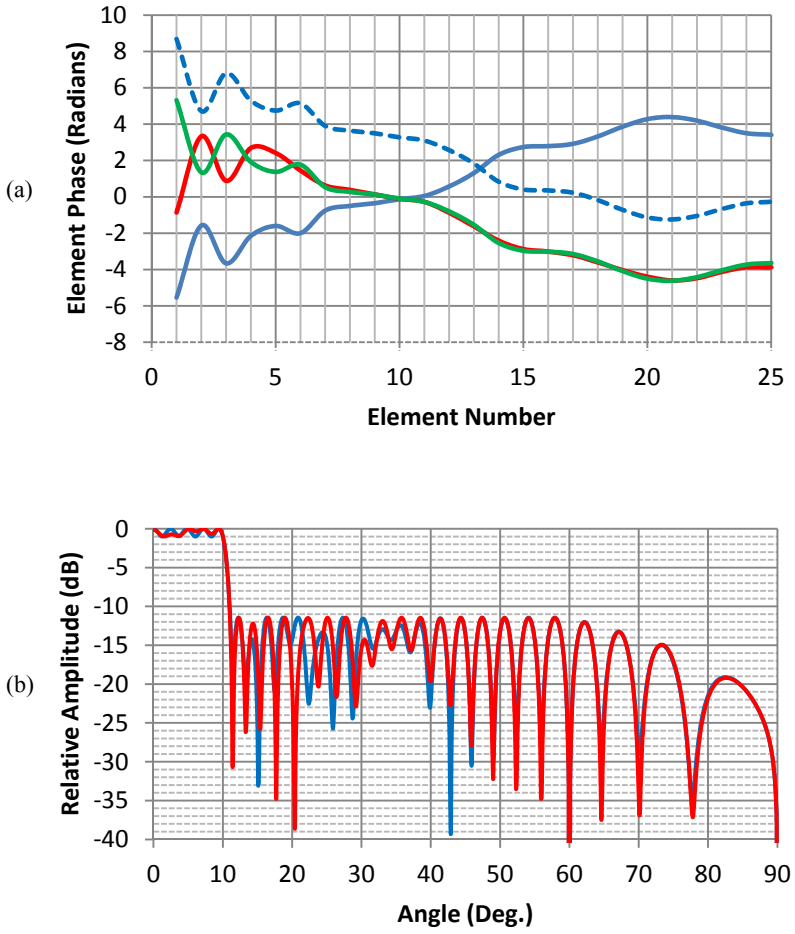

Fig. 10 — (a) Two optimized element phase sets for ±10° flat-tops using different initial values shown in blue and red. Translating the supplement of the blue phase values (shown in green) reveals the two sets' close correspondence. (b) Patterns using the phase values from the red and blue sets shown in (a).

OPTIMIZATION SUFFICIENCY

Under control by an Excel Visual Basic macro, there is no limit to how many times (iterations) the Solver can be called. Nonetheless the issue of how many is enough must be addressed. Figure 11 is a record of the macro iterations, optimized in groups of 25, to optimize the phases (not the Chebyschev weights) of the 50 elements equally spaced λ/2 apart. For a flat-top of ±5°, the objective was minimum sidelobes and ripple constrained to ±0.5 dB. As noted earlier, optimization is a process that is blind to the

inclusive phased array theory. Although the results of any of these are judged based on specification fulfillment and implementing the results, further improvement is not precluded. However, these results suggest strongly that further iterations are unnecessary.

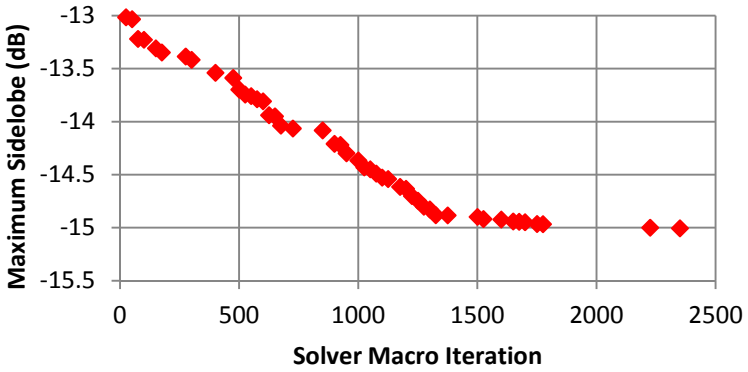

Fig. 11 — VB macro iterations for a 50-element linear array of λ/2 equally spaced elements optimized for a ±5° flat-top beam with ripple constrained to ±0.5 db. Gaps reflect iterations resulting in poorer performance (higher sidelobes) than prior best results.

Finding a demonstrable global optimum set of phases may not be feasible, or even applicable, due to applicable circuitry precision limitations, but a metric can be related to the beam pattern application. For an array transmitting with constant amplitude and phase element drive signals, the pattern is the familiar sinX/X pattern shown in Fig. 12. Here, concerns for singular target resolution favor minimum sidelobes. Therefore the maximum sidelobe or the integrated sidelobe power is an applicable metric.

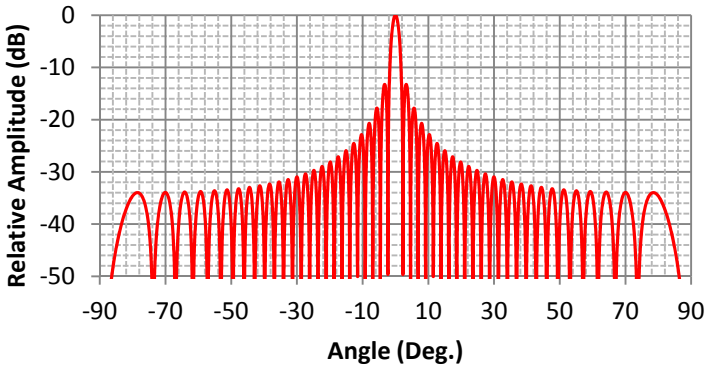

Fig. 12 — Array pattern of 50 λ/2 spaced elements without amplitude or phase variation of the element signals. The −3 dB pattern width is 2° and the first (largest) sidelobe is −13.2 dB from the pattern maximum.

Figure 13 illustrates the relationships among component powers for the array shown in Fig. 12. The power in the main lobe is defined from beam center to the −3 dB angle; the power in a transition interval, defined here as that from the −3 dB angle, that at the first pattern null (2.3°), and the remaining angular band through 90°. To maintain the equivalence with phase-only flat-top element tapering, Taylor amplitude element tapering was not applied.

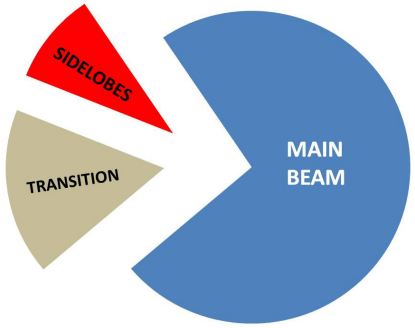

Fig. 13 — Division of integrated power among the three pattern groups for the normal nonwidened array beam shown in Fig. 12. Main beam: 73.2%; Transition: 17.3%; Remaining (sidelobes): 9.5%.

Although the angular selectivity characteristic, $\sin\theta/\theta$, is important, the character of a flat-top beam is defined less by its selectivity at the beam's edges and more by the ripple within the flat-top. Therefore, in addition to the same integrated power groups, the additional beam ripple is also important. These are included in Fig. 14 for the array plots in Fig. 6. For the wide 40° flat-top width, even the ±0.5 dB improvement in the ripple leads to a significant increase in the main beam power.

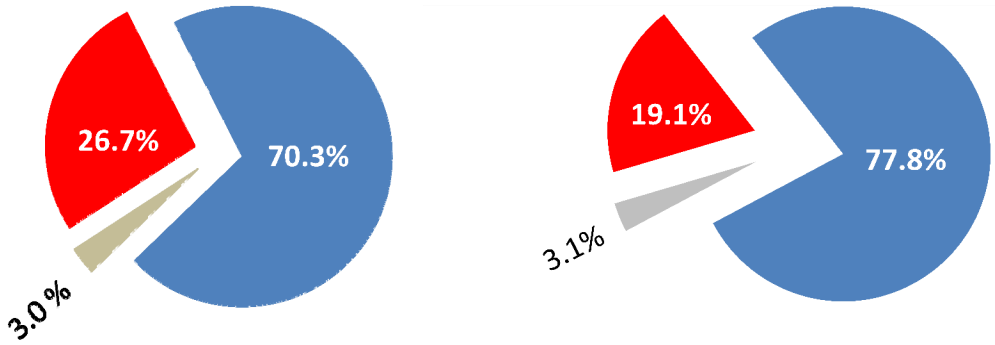

Fig. 14 — The relationships among integrated powers of the ±20° main beam flat-top (blue), transition (grey), and sidelobes (red). Left illustration is from the array pattern shown in red in Fig. 6 with a flat-top ripple of ±1 dB and the right from the pattern shown in blue with a flat-top ripple of ±0.5 dB.

Tables 1 and 2 show the detailed values used for all the red plots in Figs. 4 through 9. These relied on a ripple constraint of ±0.5 dB, which could not always be fulfilled. Nonetheless the advantage of limiting the 10 Chebyschev weights to define the 25 different element phases reduces the work considerably. As shown next, the number of array elements is nearly independent of the number of these weights.

Table 1 — Component Pattern Areas and Ripple of the Red Plotted Patterns in Figs. 4 Through 9

	±5°	±10°	±20°	±30°	±40°	±50°
Flat-Top	59.5	37.2	70.3	94.2	89.9	94.2
Transition	17.8	7.9	3.0	1.9	3.3	1.4
Sidelobes	22.8	54.9	26.7	3.9	6.8	4.4
Ripple	±1 dB	±0.5 dB	±1 dB	±1.5 dB	±1 dB	±2.5 dB

Table 2 — Component Pattern Areas and Ripple of the Blue Plotted Patterns in Figs. 4 Through 9

	±5°	±10°	±20°	±30°	±40°	±50°
Flat-Top	69.0	86.8	77.8	90.1	90.3	83.3
Transition	9.3	4.5	3.2	2.6	3.7	3.6
Sidelobes	21.7	8.7	19.0	7.2	6.0	13.1
Ripple	±0.5 dB	±0.5 dB	±0.5 dB	±0.5 dB	±0.8 dB	±0.8 dB

LARGE LINEAR ARRAYS

Expressing the array element phases in terms of even-ordered Chebyschev polynomials effectively separates the physical size of the array from determining these phases. It is convenient and fast, and alone may be sufficient. If not, it provides a good starting set for further optimizing, as described above. Consider a linear array of 200 elements spaced $\lambda/2$ apart, a very large array; in S-band this represents a length of over 30 feet, a possibly unlikely size. With equal phased elements, the −3 dB beamwidth of that array would be about 0.25°. To change the phases for a ±5° flat-top with little ripple, the optimization objective and constraint were interchanged; minimum ripple with sidelobes (beyond a 2° transition band) less than −10 dB. For 200 elements, 100 unique values, element phase values δ_1, δ_2, , , , δ_{99}, δ_{100} require definition. The 10 Chebyschev weights shown in Table 3 and the corresponding pattern in Fig. 15 required about 500 iterations of the macro, each using about 50 trial values. It was clear that no improvement would result from additional repetitions. Then using these weights, with the corresponding element phases defining an initial phase set, further optimization quickly produced the flat-top pattern shown in Fig. 15, with ripple about ±0.15 dB about the ±5° beam center. But the result would have been the same with many fewer weight optimizations and not many more optimizations of the derived phases. The basis equivalence was also tested by attempting a solution of the inverse problem, but with poor results.

Table 3 — Ten Optimized Chebyschev Weights for the ±5° Flat-Top 200-Element Linear Array

W_2	W_4	W_6	W_8	W_{10}	W_{12}	W_{14}	W_{16}	W_{18}	W_{20}
6.26124	−0.72345	−0.16951	0.62585	0.99692	0.79339	1.35673	1.05067	0.67826	0.64469

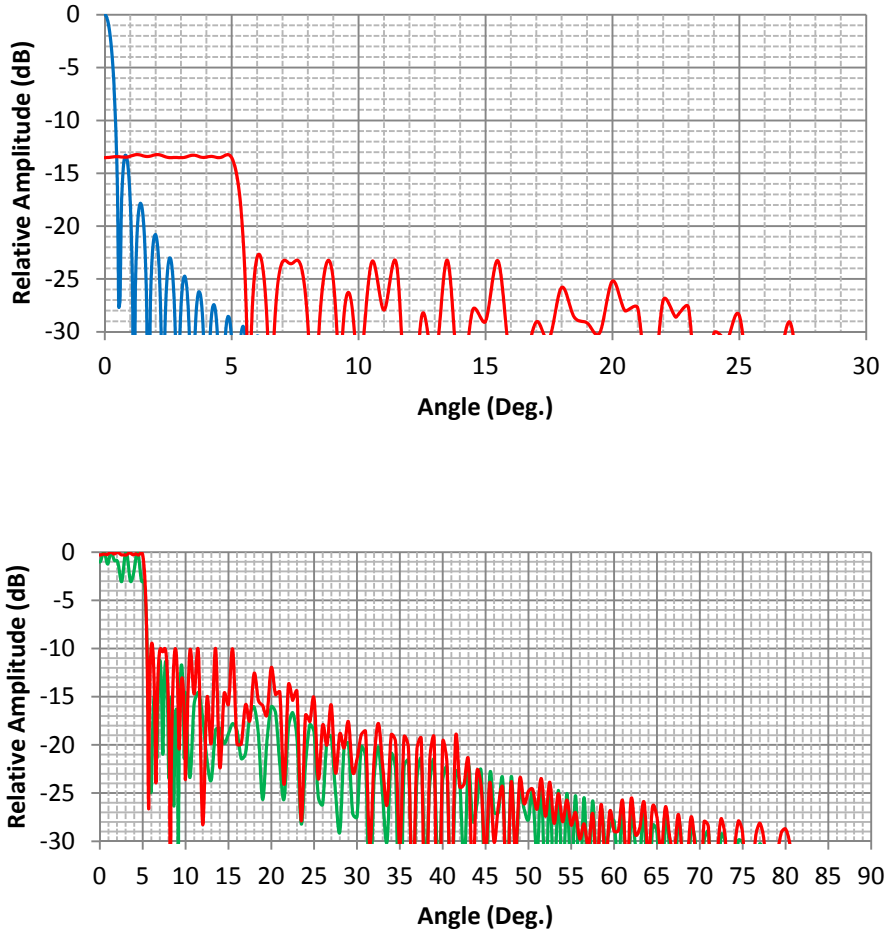

Fig. 15 — Patterns for 200 λ/2 spaced elements. Top: Expanded pattern results with and without element shape phase are shown in red and blue. Bottom: Patterns in green and red compare patterns using phases from only Chebyschev weights (green) and those with additional phase optimization (red).

PHASE BITS AND PRECISION

Array patterns have been optimized without regard to the limitations in phase shift precision. Although convenient for the analyses, any application must further consider the use of finite-precision phase-shifters. Constraints during optimization limited each of the element phase values within ±2π radians, which define degree values within the interval 0°→ 360°. For an n-bit phase-shifter, assuming a maximum interval of S = 360°, the least significant bit (LSB) is simply given by

$$LSB = \frac{S}{2^n}.$$

Therefore the LSB for a 6-bit phase shifter is 5.625°; for 5 and 4 bits these are 11.25° and 22.5°, respectively. Successive bits then increase the degree equivalents by these same amounts. The default precision of Solver is 14 to 16 places beyond the decimal point, so only the quantization introduced by actual phase shifters is significant in terms of the differences within a ±90° angle interval. A comparison between the optimized values for a ±10° flat-top and the 4-bit equivalent values is shown in Fig. 16. Numerical phase differences actually vary between −6% and +8%, although little difference is evident on the scale of this figure. Figure 17 compares the flat-top region using the optimized phase values with another using the closest 4-bit values. It has been found that while repeated optimizations were necessary to reach an acceptable plateau as shown in Fig. 11, the subsequent 4-bit approximations should be adequate based on the three detailed beamwidth regions shown in Table 4. This somewhat surprising result is due to a combination of the large numbers of elements and the round-off process which effectively introduces additional random phase variations.

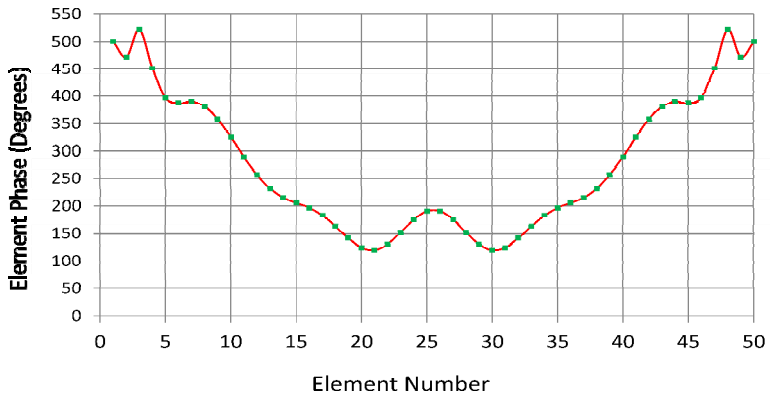

Fig. 16 — Optimized element phase distribution (red) and the closest 4-bit values (green) for the ±10° flat-top linear array

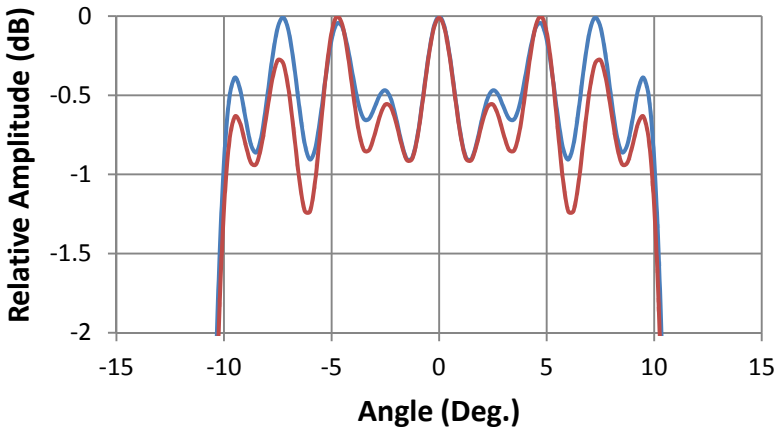

Fig. 17 — Details of the ±10° regions, using the optimized phases (blue) and the closest 4-bit approximations (red), confirm little difference in the ripple

Table 4 — Field Divisions for a ±10° Flat-Top Pattern Using Optimized Phases and Their 4-bit Approximations

	Optimized	4-bit Equiv
Flat-Top	86.8%	87.2%
Transition	4.5%	4.3%
Sidelobes	8.7%	8.5%

FLAT-TOP BANDWIDTH

So far, all the analyses and the resulting patterns have depicted performance, primarily main-beam ripple and maximum sidelobe level, assuming monochromatic signals. Element phases are optimized based on a fixed inter-element spacing. However, in a real signal environment, neither of these is static. Device phase shifters can be wideband, but still finite, and equivalent shifts using time sequencing, e.g., a CORDIC algorithm, are not. In terms of the basic electromagnetic equation on p. 3, element spacing is basically a frequency-dependent or wavelength-dependent function. In terms of overall flat-top characteristics, the optimized results show that frequency changes can greatly impact the flat-top pattern width, with very little impact on the maximum sidelobe level. Figure 18 illustrates the results for the nominal ±10° pattern using the same data used for the pattern on Fig. 5.

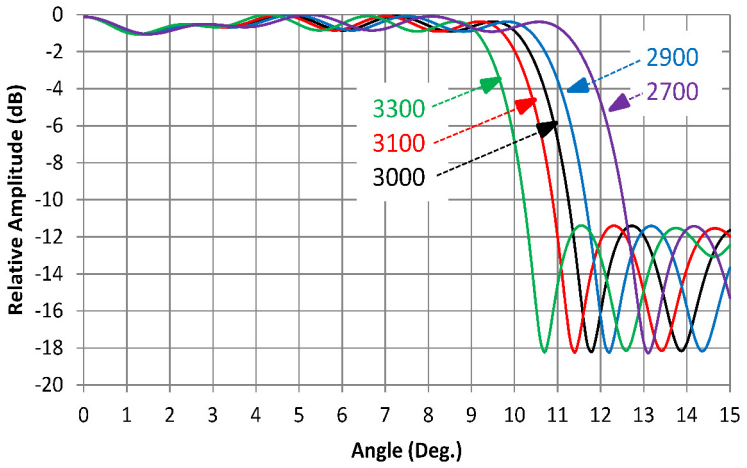

Fig. 18 — ±10° flat-top main-beam characteristics for the linear array of 50 elements spaced λ/2 apart at 10 cm (3000 MHz). Element phase shifters are assumed wideband; only equivalent frequency-dependent inter-element spacing is considered.

FLAT-TOP BEAM SCANNING

Scanning any beam from an array requires adding a phase gradient across the aperture so that the signal from each of the elements, in addition to that for the beam shape, is in-phase at the desired LOS pattern plane angle. Figure 19 illustrates the association of the phase variations which defines the array pattern together with the steering phase gradient. For element spacing λ/k and a flat-top beam steering angle γ, the element array steering phases are

$$\beta d'_n = \frac{2\pi}{k}(n-1)\sin\gamma,$$

and the LOS pattern plane phases for N even number of elements is

$$\beta d_n = -\frac{\pi}{k}(N+1-2n)\sin\theta.$$

The sum of these and the symmetric flat-top shaping phases, defined by $\delta_{N+1-n} = \delta_n$, define the pattern of the flat-top beam with its center offset by angle γ.

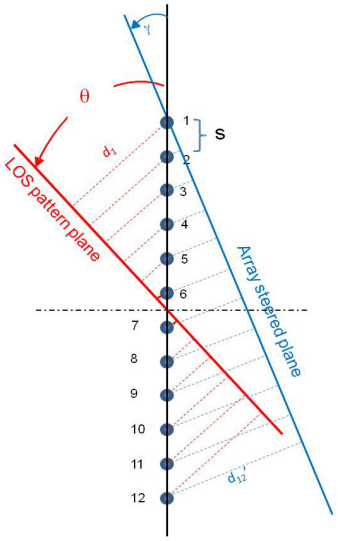

Fig. 19 — Linear element array and phase distances to the array steered angle γ and the LOS antenna pattern plane. Their combined phases together with the flat-top shaping phases define the complete steered pattern.

The resulting patterns for a ±10° flat-top steered to −10°, −20°, and −50° are shown in Fig. 20. Without further correction to the shaping phases, the offset beams widen with increased scan due to the reduced effective array aperture. Some degradation in the ripple and flat-top slope is also experienced, although further steered angle-dependent element phase correction can be applied if needed.

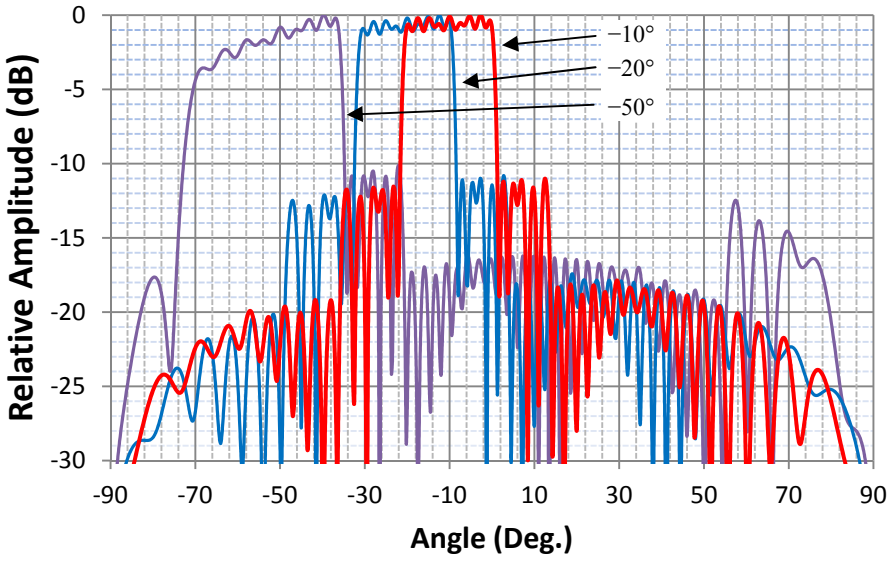

Fig. 20 — Patterns for the ±10° flat-top (red) steered to −10°, −20°, and −50° exhibit the effects of reduced effective aperture and degradation of the flat-top characteristics

PLANAR ARRAY LATTICE GRIDS

Combining flat-top beam parameters of two orthogonally oriented linear arrays effectively characterizes the 3D beam performance for an array with a rectangular or triangular grid lattice. As viewed in the plane of the two linear arrays, the lattice can take several commonly used forms, as shown in Fig. 21. These consist of evenly divided rows and columns or evenly staggered rows of elements.

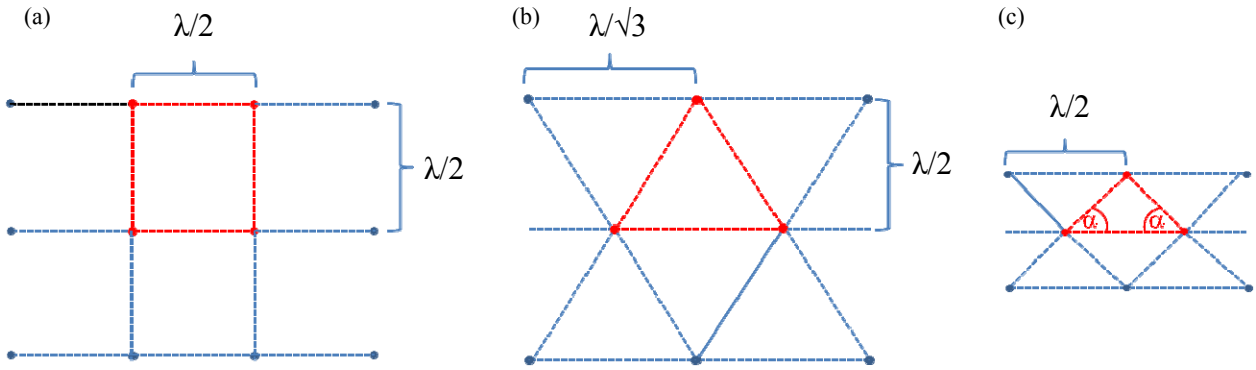

Fig. 21 — Commonly used array lattice grids use equally spaced element rows and equally spaced or staggered columns. (a) square lattice; (b) hexagonal or equilateral triangular lattice; (c) isosceles triangular lattice. For a specific aperture size, fewer elements fill the aperture using lattice (b), while lattice (c) requires more elements and enables greater radiated power.

Triangular lattices can form isosceles triangles with corner angles of 30° and 45°, or equilateral triangles (sometimes termed hexagonal) with corner angles of 60°. Then the entire array can be aligned with the X-Y axes or at an angle of 45°. Element spacing within the lattice often depends on avoiding the grating lobes, basically the repetitive nature of the array pattern within the visible angular space of the array, and is described in detail by Rudge, Milne, Olver, and Knight [14]. Other selections involve the number of elements covering an array surface, since it is possible to reduce these by about 15% using the equilateral triangular lattice. Conversely, for a transmit array, tighter packing enables greater radiated power. The pattern synthesis using any of these lattices is the same. Each is determined by the phase shaping distribution along two orthogonal directions together with the element location within the lattice. Although readily visualized, this approach is not essential. Laxpati and Shelton [15] considered combining canonical forms of two-dimensional array sets.

ARRAY LINE-OF-SIGHT PLANE

Optimized pattern synthesis is with respect to an array in the X-Y plane of a Cartesian coordinate system as illustrated in Fig. 22. The LOS plane is normal to the line OP_O defined by the elevation and azimuth angles φ and θ, and is at a range R. Its equation is defined by intercepts with the axes, which can be determined as illustrated in Fig. 23. The intercepts are then $u_X = R/\sin\phi$, $u_Y = R/(\cos\phi\sin\theta)$, and $u_Z = R/(\cos\phi\cos\theta)$.

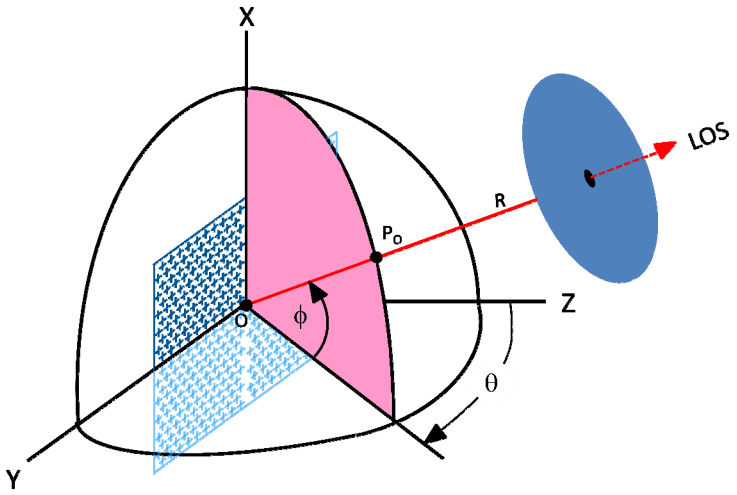

Fig. 22 — Cartesian coordinates defining the line-of-sight (LOS) plane in terms of azimuth (θ) and elevation (φ) angles relative to the array in the X-Y plane

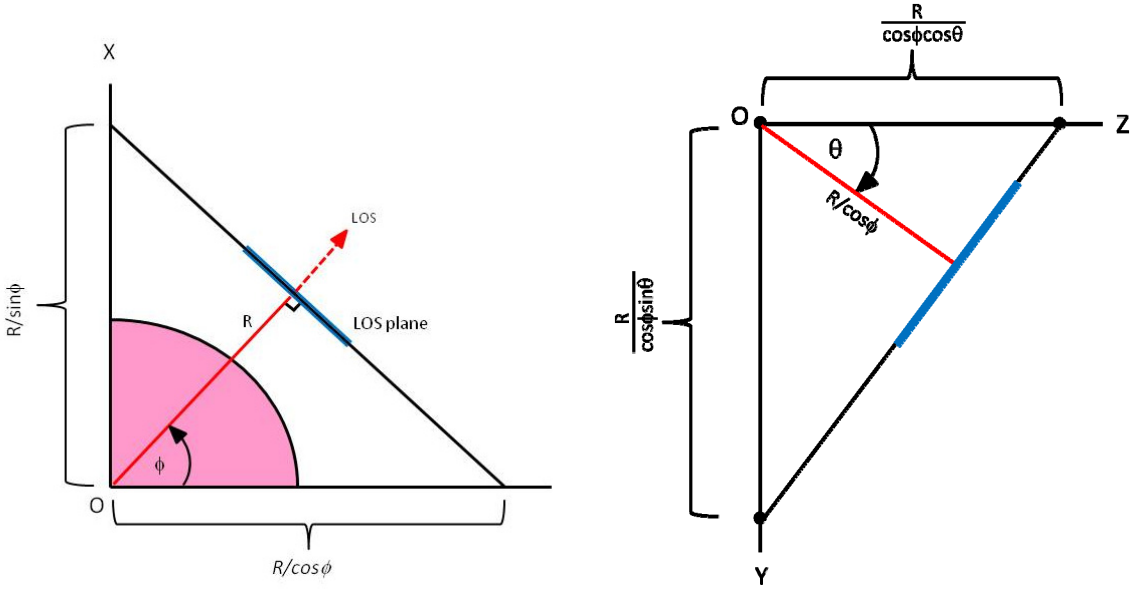

Fig. 23 — Left: the intercepts of the LOS plane with the O-X axis and the Y-Z plane. Right: the intercepts of the LOS plane with the Y-Z axes.

The general form of the equation of a plane in terms of these intercepts is

$$\frac{x}{u_X}+\frac{y}{u_Y}+\frac{z}{u_Z}=1 \ .$$

The LOS plane in terms of the axes intercepts is then

$$x\sin\phi + y\cos\phi\sin\theta + z\cos\phi\cos\theta - R = 0 \ .$$

This is also in another generally used form $Ax + By + Cz + D = 0$.

The distance from any point x_n, y_n, z_n in the array plane to the LOS plane in terms of these A, B, C, D parameters is given by the familiar form

$$d_n = \frac{\left|Ax_n + By_n + Cz_n + D\right|}{\pm\sqrt{A^2 + B^2 + C^2}} ,$$

in which the radical sign is opposite to that of D. Then for points in the array, with $z_n = 0$,

$$d_n = \left|x_n \sin\phi + y_n \cos\phi\sin\theta - R\right| .$$

Assuming R is much larger than the array, all lines from the array to the LOS plane are parallel. Since the phase of the field from every array element in this plane is $\beta d_n = \frac{2\pi}{\lambda} d_n$, the common phase βR can be ignored from the total amplitude which is then just the total of the N complex phase terms:

$$E = \sum_{n=1}^{N} \varepsilon^{j\beta d_n} \ .$$

REPRESENTATIVE 3D PATTERNS

The array pattern is a complex sum of three phase groups (or equivalent time delays): the flat-top shaping phases, the beam steering phases, and the phases representing the equivalent distance of each element to a LOS pattern observation plane, detailed in the previous section. Common to all antennas, the projected aperture area when the array is steered off the central array axis (OZ in Fig. 22) is reduced. Therefore without specific compensating changes in the shaping phases, the flat-top width will increase

but the sidelobes will decrease, a useful characteristic in reducing radar reflected clutter power. Principal plane patterns, each without azimuth or elevation steering, are shown here, but a diagonal plane (often termed intercardinal) pattern cut readily shows these changes.

Assuming a square grid array lattice illustrated in Fig. 21(a), a 2500-element array using 50 λ/2 equally spaced elements along the X and Y planes for a ±5° flat-top can each use the same list of optimized phases, as shown in Appendix A. Within the array grid, the phase of each element is the sum of values according to their row and column location. Figures 24 through 26 show the results.

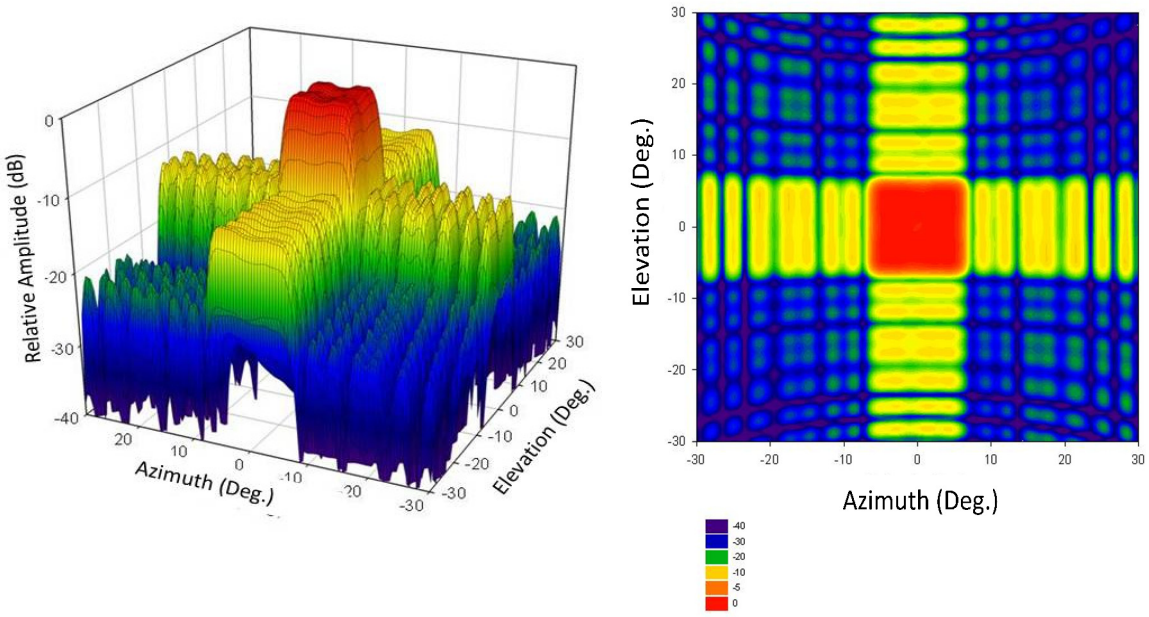

Fig. 24 — Array pattern for a ±5° flat-top array of 2500 elements of 50 equally spaced λ/2 elements along each of the X and Y axes illustrated in Fig. 22. The pattern is characteristic of the square grid lattice array.

The planar view pattern in Fig. 24 retains the expected square profile throughout the angular coverage. This is also shown in the single array pattern cuts in Fig. 25. As expected, these two patterns are essentially identical. The diagonal cut in Fig. 26, when the azimuth and elevation angles are combined along the diagonal, shows the widened flat-top and much lower sidelobes. To take advantage of this effect, which is independent of the shaping phase, the entire array has sometimes been simply rotated by 45° about the central axis OZ shown in Fig. 22.

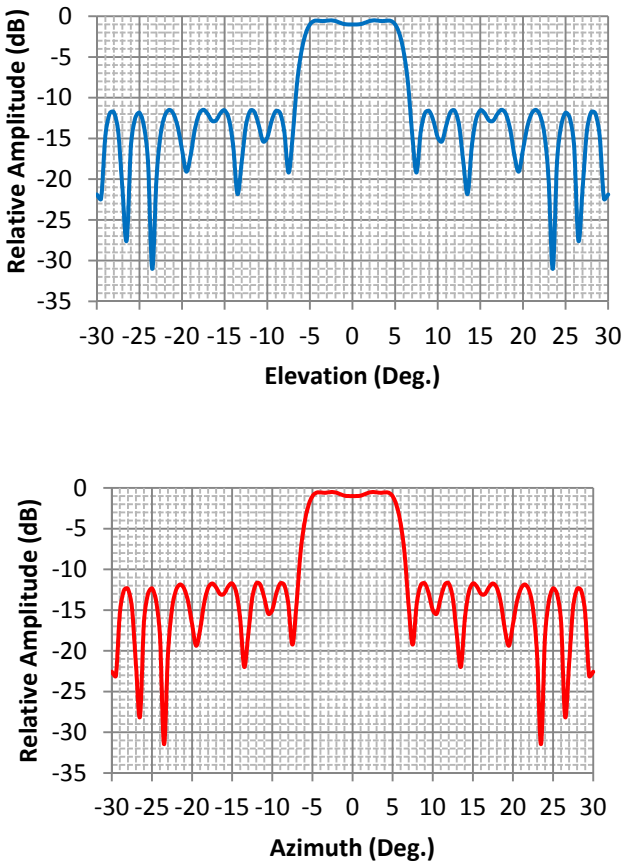

Fig. 25 — Patterns of a 2500-element square grid lattice array with equal λ/2 row and column spacings. Top: Elevation pattern at 0° azimuth. Bottom: Azimuth pattern at 0° elevation.

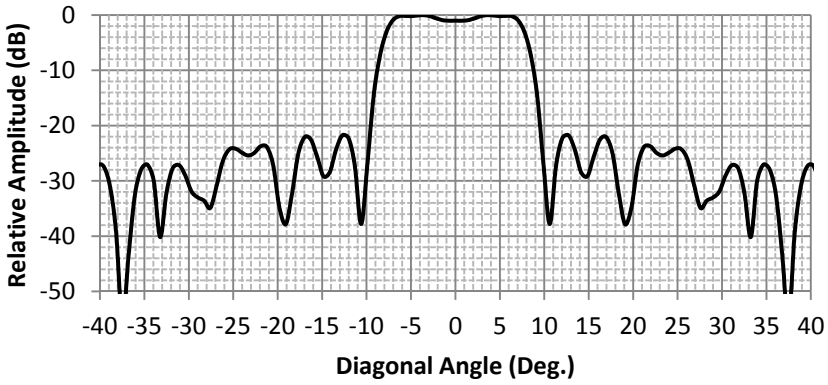

Fig. 26 — Diagonal (intercardinal) pattern cut of the same array as shown in Fig. 24. For a flat-top, the beam width is increased, but the sidelobes are substantially decreased along this direction.

Assuming phase-only pattern shaping, the square gridded array lattice always results in a square profile about the principal array normal. Several of these, for different flat-top widths using the same 2500-element lattice, are shown in Figs. 27 through 31, and their parameters listed in Appendix A.

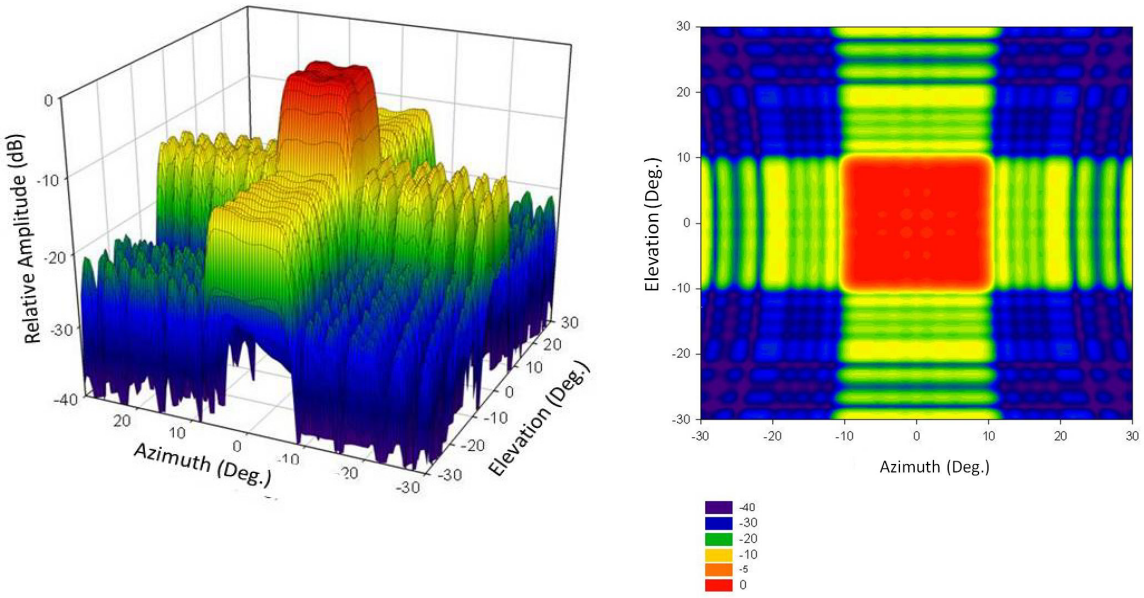

Fig. 27 — Patterns of a phase-only 2500-element square lattice array optimized for ±10° pattern with ±0.5 dB ripple. All elements are separated by λ/2.

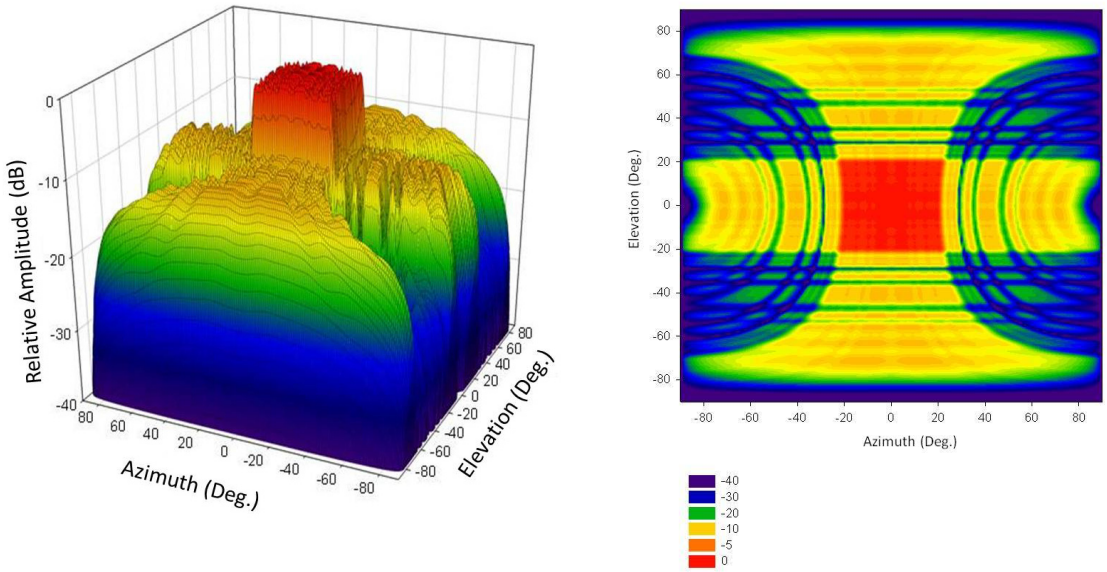

Fig. 28 — Same 2500-element array with element phases optimized for a ±20° flat-top. Note the patterns show the coverage over the complete ±90° in azimuth and elevation, revealing the effect of aperture reduction at wide angles. The distortion has very little effect on the relatively small flat-top.

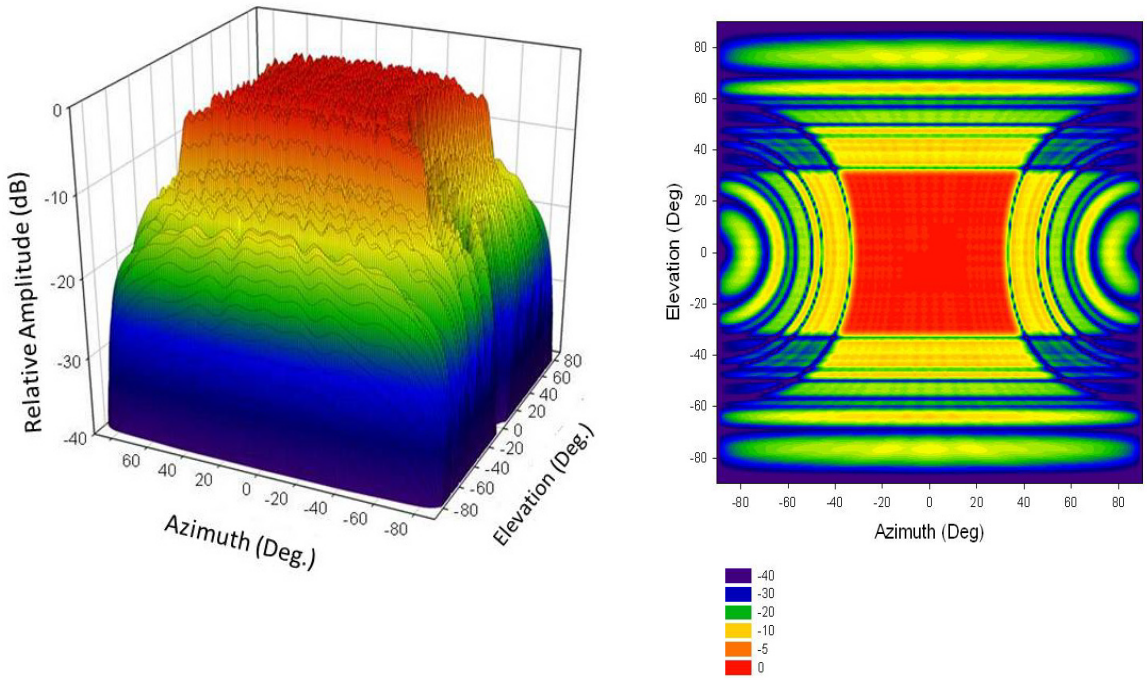

Fig. 29 — Element phase shaping of the 2500-element array changed to synthesize a ±30° flat-top. The square pattern is again distorted, but the effect is evident in the main flat-top beam as well.

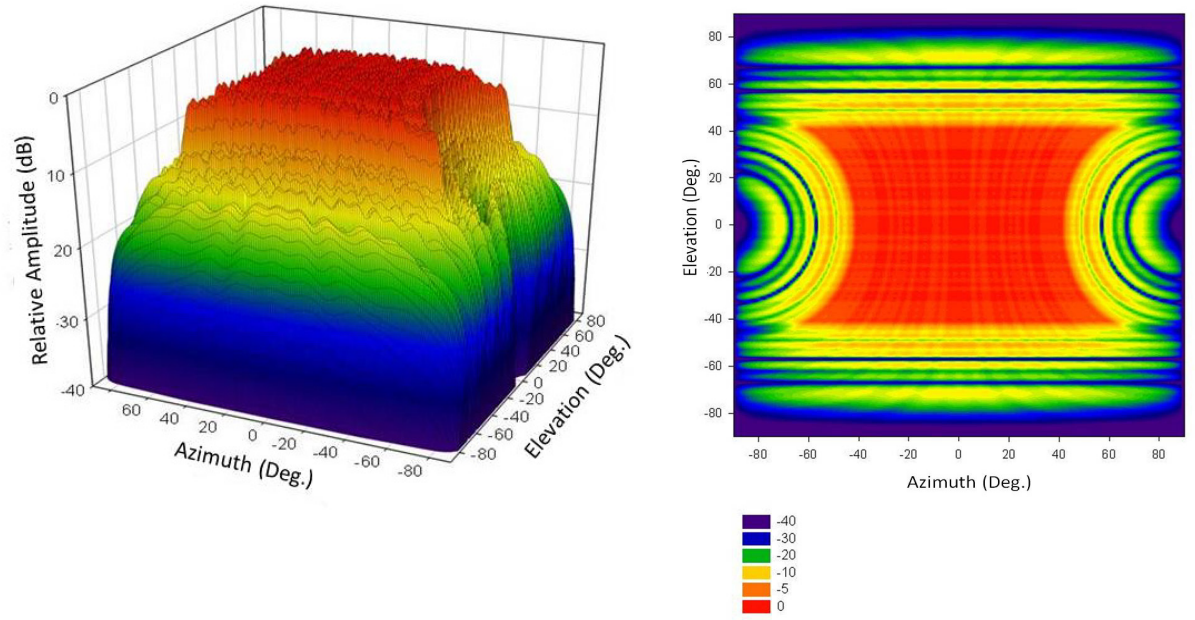

Fig. 30 — Element phase shaping changed to synthesize a ±40° flat-top for the 2500-element array. In addition to the distortion due to the wide angular coverage, the main-beam ripple is greater.

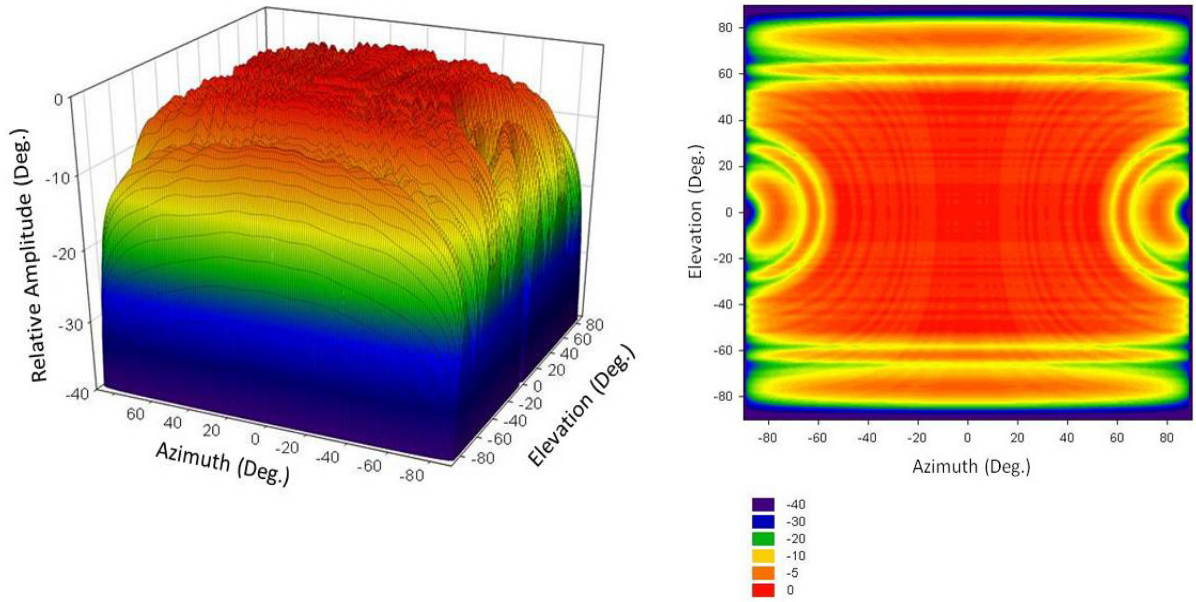

Fig. 31 — Element phase shaping changed to synthesize a ±50° flat-top for the 2500-element array. In addition to the distortion effects, the main-beam ripple is greater and the sidelobe levels significantly higher.

The results for arrays with an equilateral triangular grid lattice (vertical element spacings of λ/2 and horizontal element spacings of λ/√3) are similar for square profile flat-tops, as shown in Fig. 32 for a ±10° flat-top.

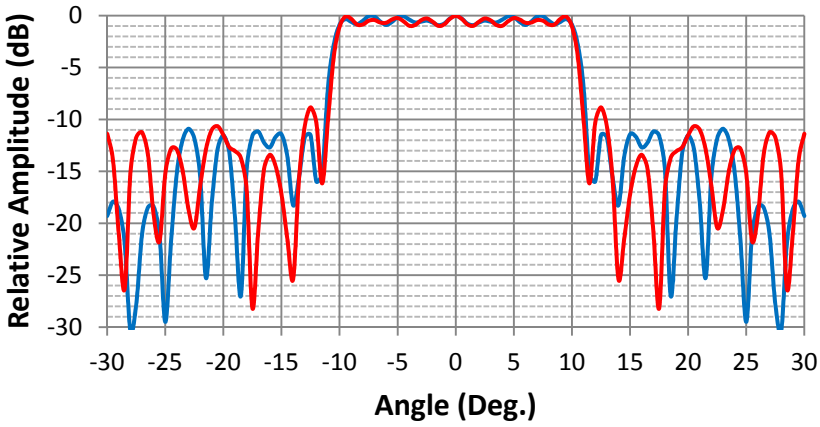

Fig. 32 — Principal plane cuts for a ±10° flat-top using a hexagonal grid array. "X" and "Y" element spacings: λ/2 and λ/√3, respectively. With azimuth at 0° the elevation is shown in red; with elevation at 0° the azimuth is shown in blue.

Rectangular profile flat-top patterns can also use the same method as the square profile flat-top beams. Figure 33 illustrates the results for a rectangular array of 2500 elements arranged in an equilateral (hexagonal) array matrix. For a profile ±10° azimuth and ±5° elevation, the phase of each element, using the optimized single row element values, is the sum of these values in row-column order.

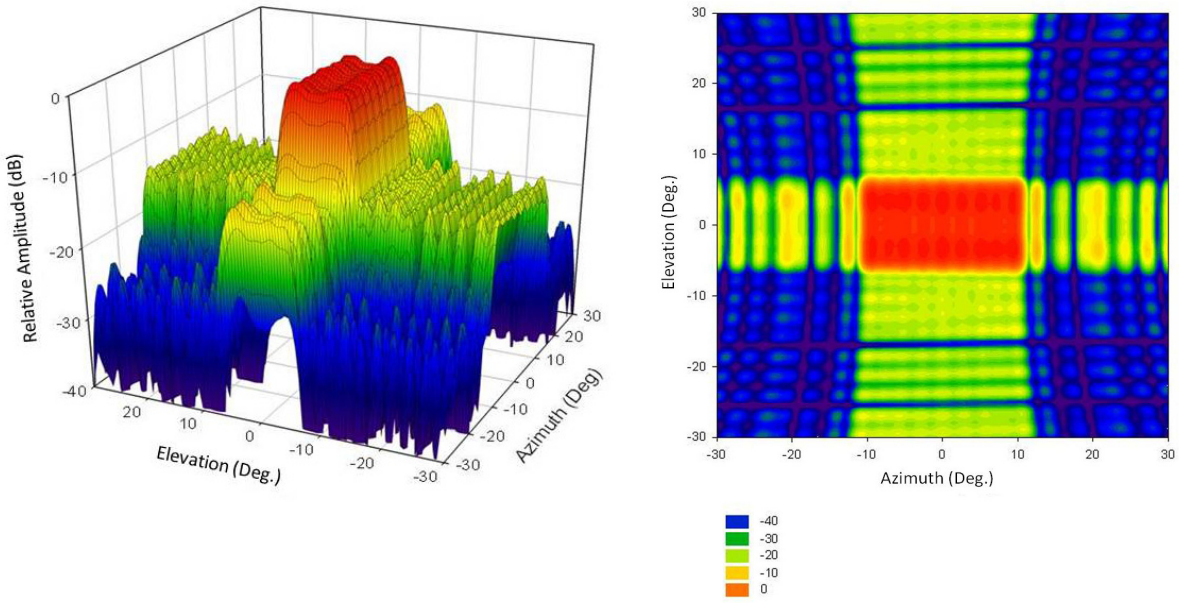

Fig. 33 — Rectangular profile patterns for a 2500-element rectangular array using an equiangular triangular grid. Elements are spaced λ/2 apart vertically and λ/√3 horizontally. Ripple is constrained to ±0.5 dB.

However, there is a trade-off in the optimization process between the maximum beam sidelobes and the flat-top ripple. The result is clearly shown in Fig. 34. Although each profile may be acceptable, the normalization of the combined profile parameters results in a distinguishable amplitude difference in their maximum flat-top levels.

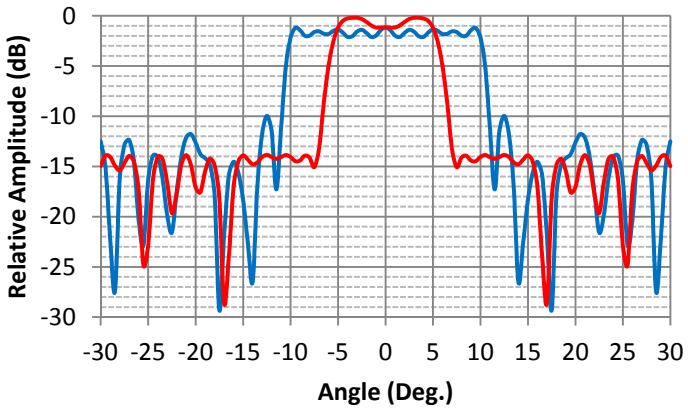

Fig. 34 — Principal elevation and azimuth plane pattern cuts for the rectangular profile flat-top pattern in Fig. 33. The ripple within each flat-top is about ±0.5 dB. The difference in average amplitude in each plane is due to the difference between the two pattern widths.

CIRCULAR FLAT-TOP PATTERNS

The array lattices illustrated in Fig. 21 are essentially rectangular, albeit some triangular with displacement of alternative rows. Using only element phasing, it is then not surprising that the patterns result in the square or rectangular profiles shown in the previous section. Other profiles also need to be developed. For example, Fig. 20 illustrates the effect of angularly scanning an otherwise square flat-top beam. During scanning, the effective array aperture is progressively decreased, resulting in differential amplitude changes that effectively tilt the beam top. Here, except for some reduction in the width of the flat-top, correcting this amplitude slope can be accomplished with a change in the element phase distribution within the array lattice. However, another issue remains concerning the actual profile of the beam. Can circular or other non-rectangular flat-top profiles also be generated? The short answer is "no," primarily due to the geometry of the array grid lattice.

Simply applying the same linear single row phase shape profiles to both orthogonal axes results in a square profile flat-top. A circular profile can be synthesized, but ideally requires a radial and circularly symmetric phase shape profile. The difficulty that must be overcome is the element pattern grid. Compare the two illustrations in Figs. 21(a) and (b). Each use the same square and triangular grids as illustrated in Figs. 35(a) and (b), but with an added suggested isophase ring structure. Ring phases can then be derived in the same manner as the linear element phases.

Clearly, radial symmetry is not possible with either grid, although the element locations as shown in Fig. 35(a) could be considered similar to a concentric circular ring structure, so using flat-top optimized linear array values, either calculated, extrapolated, or even further optimized, is reasonable.

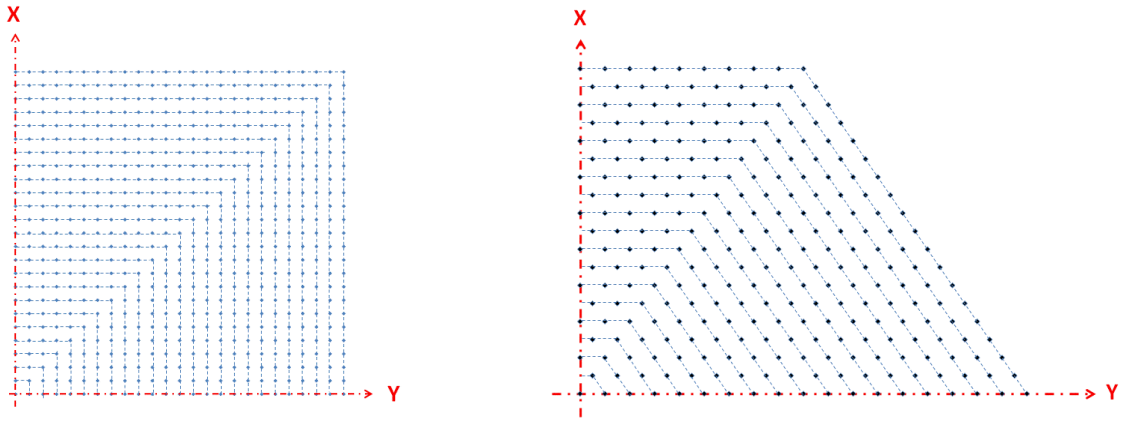

(a) (b)

Fig. 35 — (a) One quadrant of a 2500-element square grid array with elements spaced λ/2 apart. Twenty-five concentric square "rings" can define element phase shaping. (b) One quadrant of a 1027-element array with elements spaced λ/2 and λ/√3 apart forming an equal angular (hexagonal) grid. Eighteen concentric hexagonal "rings" can define element phase shaping.

Unfortunately the results are patterns similar to the one shown in Fig. 36. Optimizing phase tapering based on an approximated circular ring structure or the actual array radial distances does enable a widened circular beam profile, but is an obviously unacceptable flat-top.

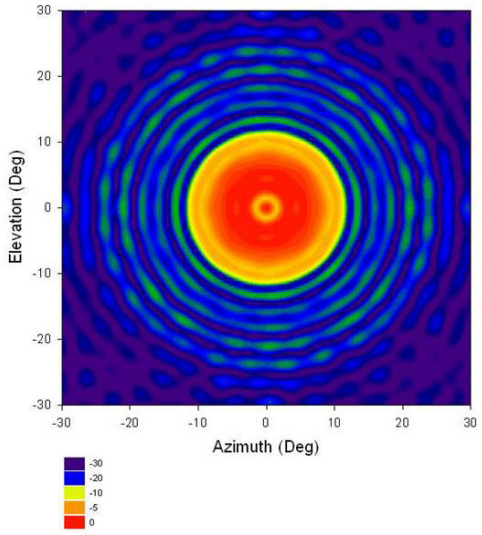

Fig. 36 — Optimized ±10° flat-top pattern using element phases from a square or rectangular grid lattice. The widened pattern retains a central ring similar to one with equal element phasing.

Recently, McPhail, Coleman, and Scholnik [16], using primarily an analytic approach rather than the total optimization approach, show similar results, although the goal was not a flat-top pattern. An alternative, choosing extrapolated phases based on the actual radial location of each element in the array, rather than approximated circular concentric rings, produces the same result.

Using a triangular or hexagonal grid lattice offers another possibility, implied by the array lattice shown in Fig. 35(b), again with a suggested isophase ring structure of concentric inscribed λ/2 spaced rings. Obviously, elements in the outer array corners must be excluded, but each of the others can be associated with a closest ring. Identifying the 25 concentric rings of a 25 × 25 square element array matrix, and using appropriate shaping phases, the result applied to a ±10° flat-top are shown in Fig. 37, again unacceptable.

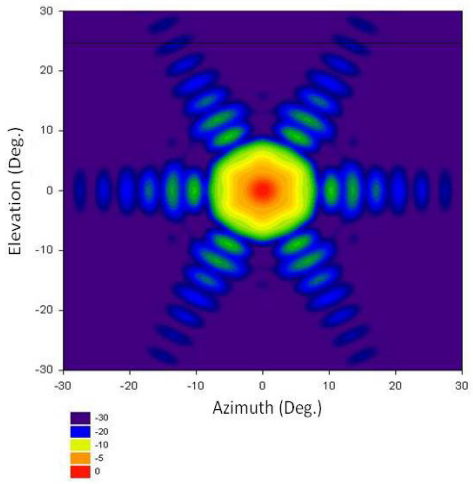

Fig. 37 — Optimized ±10° flat-top pattern using the hexagonal grid of Fig. 35(b). The widened pattern retains structure that includes a central ring.

Another alternative uses the same radial element phase shaping, but with a *concentric circular grid lattice* rather than a rectangular or hexagonal grid. A quadrant of this array grid using 20 concentric rings is shown in Fig. 38. Rings are spaced λ/2 apart, as are elements within each ring. Although inconvenient using *contemporary* element feed structure, its application here is readily shown. This array matrix grid has been suggested before and is described in some detail by Elliott [17]. But applied to phase-only flat-top pattern development, equal radial element phase shaping assures a circularly symmetric pattern, and using a concentric ring array removes the nonuniformity noted before.

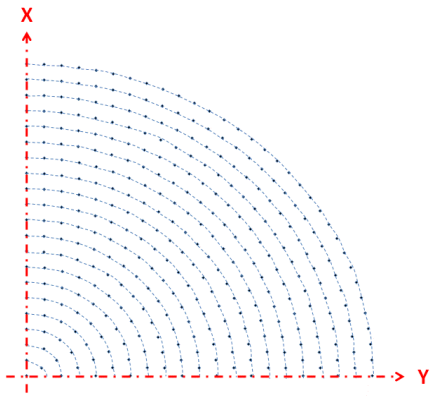

Fig. 38 — One quadrant of a concentric array grid. Elements are located in circular rings λ/2 apart and approximately λ/2 apart within each ring. 1299 elements fill a 20-ring array.

Consider a group of n concentric rings of elements spaced λ/2 apart. The circumference of the nth ring from the array center is $c_n = n\pi\lambda$. Assume all the elements in that ring are spaced at least λ/2 from all those in an adjacent ring. Next consider the number of elements within a ring; assume they too should be at least λ/2 apart. This implies a total of $2n\pi$ elements in the *n*th ring. Since only an integer number of elements in a ring are possible, this number must be rounded down to an integer value. The parameters for a 20-element circular grid ring array are shown in Table 5.

Table 5 — Parameters for a 20-Element Circular Ring Array

Ring	Radius (λ)	Number/ring	Spacing (deg)	Spacing (λ)
1	0.5	6	60.00	0.52
2	1.0	12	30.00	0.52
3	1.5	18	20.00	0.52
4	2.0	24	15.00	0.52
5	2.5	30	12.00	0.52
6	3.0	36	10.00	0.52
7	3.5	42	8.57	0.52
8	4.0	50	7.20	0.50
9	4.5	56	6.42	0.50
10	5.0	62	5.80	0.50
11	5.5	68	5.29	0.50
12	6.0	74	4.86	0.50
13	6.5	80	4.50	0.51
14	7.0	86	4.18	0.51
15	7.5	94	3.82	0.50
16	8.0	100	3.60	0.50
17	8.5	106	3.39	0.50
18	9.0	112	3.21	0.50
19	9.5	118	3.05	0.50
20	10.0	124	2.90	0.50

Adding a center element, the total number of elements in the complete array is 1299, each of which is separated by *at least* one-half wavelength. With all element signal phases set equally, the pattern is essentially the familiar sinX/X pattern shown in Fig. 39. Regardless of the actual phase distribution among the rings, the pattern will *always* be circular. Both element distance phases to the LOS plane and the element shape phases are circularly symmetric, which effectively removes the central ring structure that appears in Fig. 36. Control of the flat-top width is then the same as for the square flat-tops.

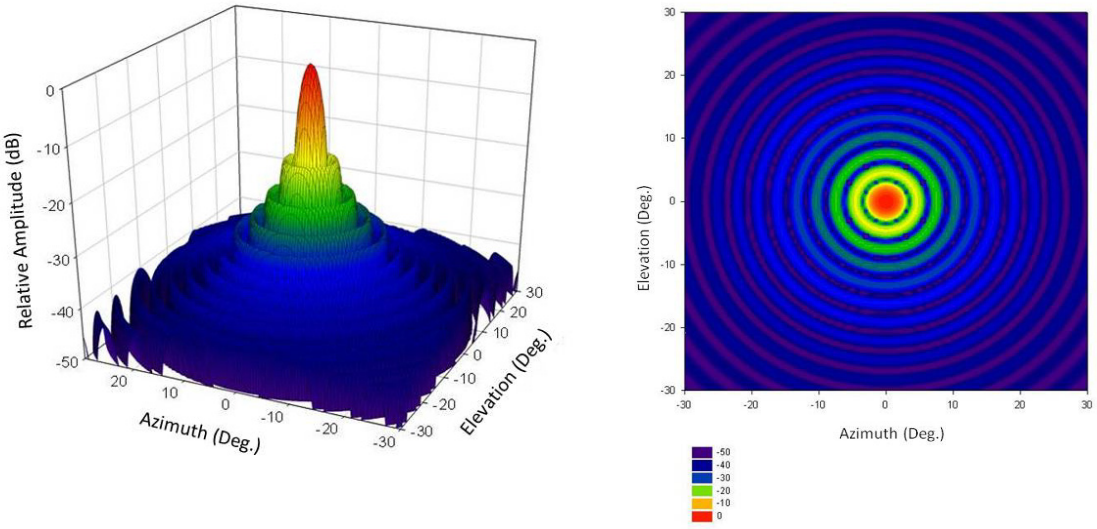

Fig 39 — Pattern using the circular concentric array, with equal phases and amplitudes of all 1299 elements, of the array illustrated in Fig. 38. Beam width and first sidelobe are similar to values of a square matrix gridded array.

Optimizing the 21 independent element phases to produce an acceptable pattern for the 41-element linear array row of λ/2 spaced elements is shown in Fig. 40. Optimization was for a pattern width of ±10° with sidelobes less than −10 dB and ripple constrained to less than ±0.5 dB.

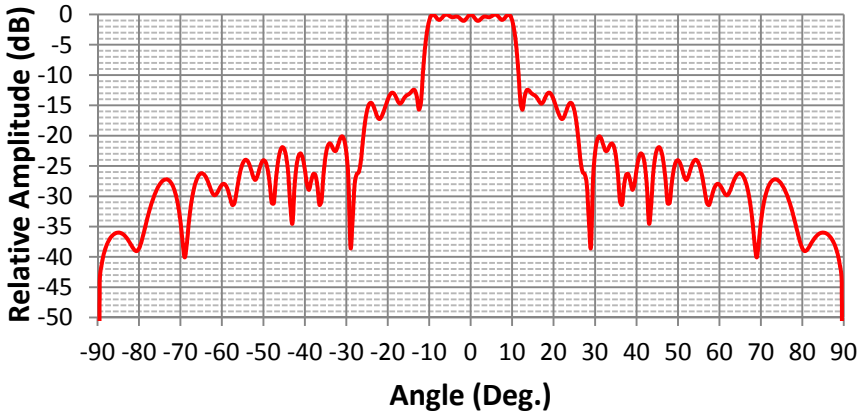

Fig. 40 — Pattern of the 41-element linear array of λ/2 spaced elements. Element phases defined those of the 20 concentric rings.

Using the element phase set that defined this pattern of the single row array to define the phases of the concentric rings, as illustrated in Fig 38, the resulting circular flat-top patterns shown in Fig. 41 fulfilled the same optimization parameters as those used for the linear array. A corresponding angular detailed plot is shown in Fig. 42. Since only 21 phase values applied to just the 20 rings and the center element of the array are involved, the association between individual elements and the shape phases is simpler than the row-column association necessary for the square flat-tops. However, this is offset analytically by the need to identify each of the circular array elements with a single one of the concentric array rings.

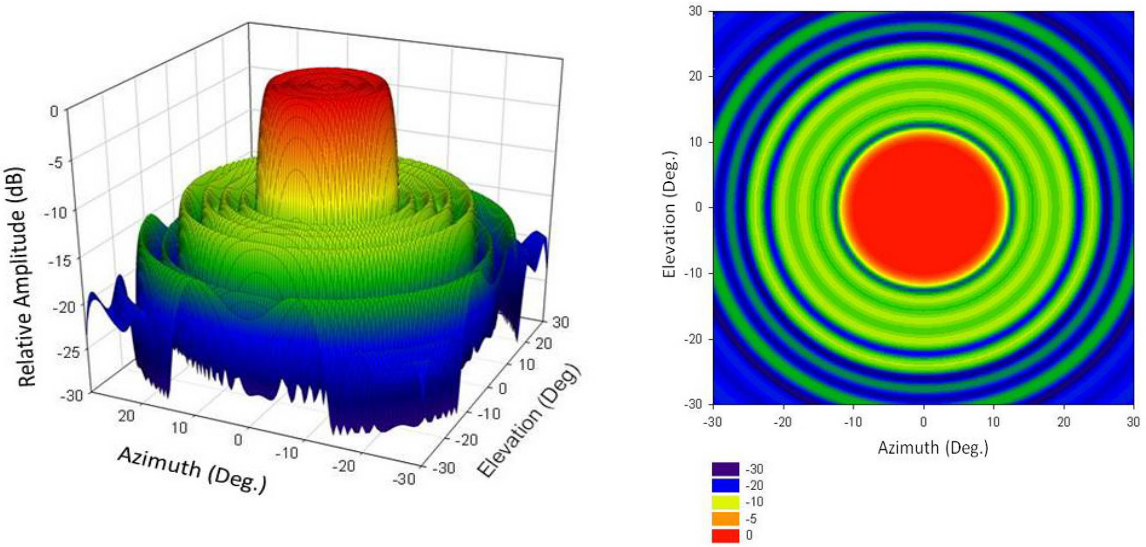

Fig. 41 — Circular flat-top using 1299 elements, nominally spaced λ/2 apart. Pattern is flat within ±0.5 dB over ±10°.

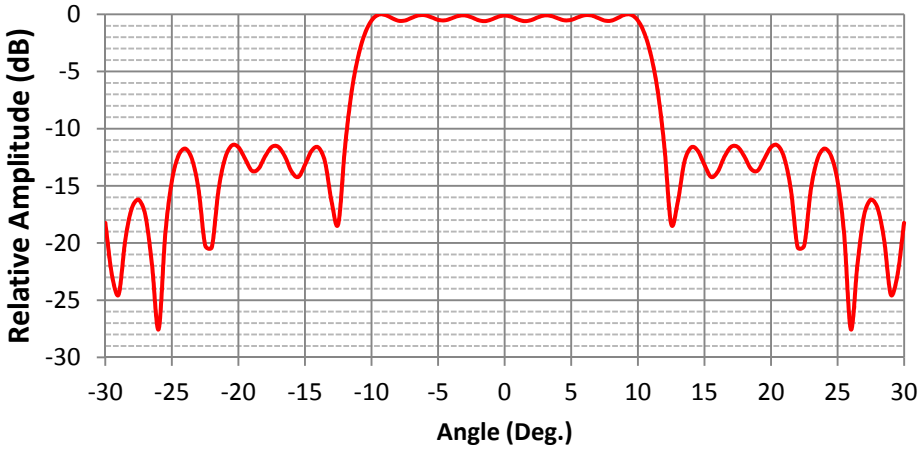

Fig. 42 — Array pattern at any angular cut of the 20-ring array patterns shown in Fig. 41

CONCLUSIONS

Array patterns with good flat-top beam characteristics that only require adjustment of the individual element phases can be readily designed. The equations are simple, but the number of variables favors an iterative optimization approach for solution. Non-iterative methods, such as those described by Laxpati and Shelton [17], while promising, do not address the requirements specific to the sector patterns described here. A wide range of iterative methods are available, many of preeminence in the current literature. Nearly all are effectively independent of the array technical details, since an acceptable solution can be defined in terms of a basic objective parameter within some defined constraints and is always recognizable. Sometimes the differences are in the convergence speed, sometimes in the precision. In this report, the results use the reduced gradient optimization technique readily available in Excel's Solver. Optimization goals were primarily minimum sidelobes within a constrained amount of flat-top ripple, although the converse was also shown. Repetitive optimization using a Visual Basic macro enabled comparison of possible new sets with candidate sets for acceptance within the defined limits. Working with large array structures is facilitated by initially optimizing a comparatively small set of Chebyschev weights with the element phases as a function of the arguments. If necessary the resulting phase set can then be further optimized starting with those phases.

Since the optimization process is essentially blind to the underlying electromagnetic array theory, the results are very much dependent on the starting phase set. As a result, different initial sets can result in differing optimized sets, any of which can be equally acceptable. When the results from different initial sets produce closely similar patterns, it may be possible, although not necessary, to demonstrate their equivalence. The relationship between the optimum shape phases and their representation in terms of the Chebyschev polynomials basis set, while appropriate to the approach described, is not very precise.

The organization of the array grid materially impacts the ripple of the flat-top beam. Those organized in a square or triangular grid are suited to beams with square or rectangular beam profiles, while an array with a concentric circular grid is required for beams with good circular flat-top circular profiles.

ACKNOWLEDGMENTS

Phase-only array pattern design using a variety of techniques is scattered throughout the literature. Work described here started in connection with the Naval Research Laboratory Radar Division's EEDAR (Every-Element Digital Array Radar) project, presently renamed FlexDAR (Flexible Digital Array Radar). Much of the basic work fulfilled the initial requirements in terms of pattern width, flatness, and sidelobe level. However, questions posed by Jim Alter concerning the more general character of flat-top patterns, especially those with truly circular profiles, although outside the immediate project requirements, offered a significantly greater challenge and an opportunity. Later, informal discussions with Dr. Merrill Skolnik, my former supervisor as a government employee, posed the likelihood of deleterious frequency effects. Addressing both of these made this a better, more general treatment of the subject. The author prepared this report while under contract with the Naval Research Laboratory, Washington, D.C.

REFERENCES CITED

1. J.H. Holland, *Adaptation in Natural and Artificial Systems* (University of Michigan Press, Ann Arbor, 1975).
2. R.L. Haupt, "Phase-Only Adaptive Nulling with a Genetic Algorithm," *IEEE Trans. Antennas Propag*. **45**(6), 1009–1015 (June 1997).
3. R.L. Haupt and S.E. Haupt, *Practical Genetic Algorithms*, 2nd ed. (Wiley-Interscience, Hoboken, NJ, 2004).
4. G.K. Mahanti, A. Chakraborty, and S. Das, "Floating-point Genetic Algorithm for Design of a Reconfigurable Antenna Arrays by Phase-Only Control," *APMC2005 Proceedings.*
5. L. Ying, G. Shuxi, S. Zongzhen, and X. Liangyong, "Design of a Shaped Beam Base Station Antenna Using Genetic Algorithm," *Journal of Electronics* **20**(1), 78–80 (2003).
6. D. Marcano, F. Duran, and O. Chang, "Synthesis of Multiple Beam Linear Antenna Arrays Using Genetic Algorithms," *Antennas and Propagation Society International Symposium 2005, AP-S Digest*, Vol. 2, pp. 938–941 (2005).
7. J. Jin, H.L. Wang, W.M. Zhu, and Y.Z. Liu, "Array Patterns Synthesizing Using Genetic Algorithm," Progress in Electromagnetic Research Symposium 2006, March 26–29.
8. F.J. Ares-Pena, J.A. Rodriguez-Gonzalez, E. Villanueva-Lopez, and S.R. Rengarajan, "Genetic Algorithms in the Design and Optimization of Antenna Array Patterns," *IEEE Trans. Antennas Propag.* **47**(3), 506–510 (1999).
9. R. Abdolee, M.T. Ali, and T.A. Rahman, "Decimal Genetics Algorithms for Null Steering and Sidelobe Cancellation in Switch Beam Smart Antenna System," *International Journal of Computer Science and Security* **1**(3), 19–26 (2007).
10. J.A. Rodriduez, F. Ares, and E. Moreno, "Linear Array Pattern Synthesis Optimizing Using the Simulated Annealing Technique," *Microwave and Optical Technology Letters* **23**(4), 224–226 (November 1999).
11. W.T. Li and X.W. Shi, "An Improved Particle Swarm Optimization Algorithm for Pattern Synthesis of Phased Arrays," *Progress in Electromagnetics Research, PIER* **82**, 319–332 (2008).
12. S.J. Blank and M.F. Hutt, "Antenna Array Synthesis Using Derivative, Non-Derivative and Random Search Optimization," IEEE Sarnoff Symposium, Princeton, NJ, April 28–30, 2008, doi:10.1109/SARNOF.2008.4520115.
13. L. Marcaccioli, R.V. Gatti, and R. Sorrentino, "Series Expansion Method for Phase-Only Shaped Beam Synthesis and Adaptive Nulling," URSI (International Union of Radio Science) EMTS International Symposium on Electromagnetic Theory, 23–27 May 2004, Pisa, Italy, pp. 676–678; available at http://www.ee.bgu.ac.il/~specmeth/EMT04/pdf/session_3/3_02_05.pdf. (A more comprehensive text is in Italian.)
14. A.W. Rudge, K. Milne, A.D. Olver, and P. Knight, *The Handbook of Antenna Design*, Vol. 2, IEE Electromagnetic Waves Series 16 (Peter Peregrinus, Ltd., London, 1983).
15. S.R. Laxpati and J.R. Shelton, "Theory of Null Synthesis of Planar Arrays," *IEEE Antennas and Propagation Society International Symposium 1981*, Vol. 19, pp. 41–43 (1981), doi:10.1109/APS.1981.1148592.
16. K.R. McPhail, J.O. Coleman, and D.P. Scholnik, "Experiments in Weight Design for a Sombrero Array Pattern," NRL/MR/5320—10-9232, Naval Research Laboratory, Washington, DC, June 25, 2010.
17. R.S. Elliott, *Antenna Theory and Design*, Rev. Ed., Section 6.7, "Sampling Generalized Taylor Distributions: Circular Grid Arrays," pp. 230–233 (IEEE Press, Wiley-Interscience, Hoboken, NJ, 2003).

BIBLIOGRAPHY

Akdagli, A., and K. Guney, "Shaped-Beam Pattern Synthesis of Equally and Unequally Spaced Linear Antenna Arrays Using a Modified Tabu Search Algorithm," *Microwave and Optical Technology Letters* **36**(1), 16–20 (2003).

Branner, G.R., and B.P. Kumar, "Improved Array Sectoral Patterns by Unequal Element Spacing," *1998 IEEE Antennas and Propagation Society International Symposium, Digest* Vol. 2, pp. 764–767, doi:10.1109/APS.1998.702051.

Brown, G.C., J.C. Kerce, and M.A. Mitchell, "Extreme Beam Broadening Using Phase Only Pattern Synthesis," *Fourth IEEE Workshop on Sensor Array and Multichannel Processing, 2006*, pp. 36–39, doi:10.1109/SAM.2006.1706079.

Bucci, O.M., and G. D'Elia, "Power Synthesis of Reconfigurable Conformal Arrays with Phase-Only Control," *IEE Proc.-Microw. Antennas Propag.* **145**(1), 131–136 (February 1998).

Bucci, O.M., G. D'Elia, G. Mazzarella, and G. Panariello, "Antenna Pattern Synthesis: A New General Approach," *Proc. IEEE* **82**(3), 358–371 (March 1994).

Casimiro, A.M.E.S., and J.A.R. Azevedo, "A Unification Procedure to the Analysis and Synthesis of Antenna Arrays," *J. of Electromagn. Waves and Appl.* **19**(14), 1881–1896 (2005).

Chakraborty, A., B.N. Das, and G.S. Sanyal, "Determination of Phase Functions for a Desired One-Dimensional Pattern," *IEEE Trans. Antennas Propag.* **AP-29**(3), 502–506 (May 1981).

Chakraborty, A., B.N. Das, and G.S. Sanyal, "Beam Shaping Using Nonlinear Phase Distribution in a Uniformly Spaced Array," *IEEE Trans. Antennas Propag.* **AP-30**(5), 1031–1034 (Sept. 1982).

Chen, S., and R. Iwata, "Mutual Coupling Effects in Microstrip Patch Phased Array Antenna," *1998 IEEE Antennas and Propagation Society International Symposium*, Vol. 2, pp. 1028–1031 (1998), doi:10.1109/APS.1998.702125.

Cheston, T.C., and J. Frank, "Phased Array Radar Antennas," Ch. 7 in *Radar Handbook*, 2nd ed., M.I. Skolnik, ed. (McGraw-Hill, New York, 1990).

Coleman, J.O., D.P. Scholnik, and K.R. McPhail, "Phase-Only Tapers for Regular Planar Arrays, a Heuristic Nonlinear-FM Approach," *2010 IEEE International Symposium on Phased Array Systems and Technology (ARRAY)*, pp. 113–120, doi:10.1109/ARRAY.2010.5613383.

Corey, L.E., "A Graphical Technique for Determining Optimal Array Antenna Geometry," *IEEE Trans. Antennas Propag.* **AP-33**(7), 719–726 (July 1985).

Davis, R.M., "Phase-Only LMS and Perturbation Adaptive Algorithms," *IEEE Trans. Aerosp. Electron. Syst.* **34**(1), 169–178 (January 1998).

DeFord, J.F., and O.P. Gandhi, "Phase-Only Synthesis of Minimum Peak Sidelobe Patterns for Linear and Planar Arrays," *IEEE Trans. Antennas Propag.* **36**(2), 191–201 (February 1988).

DuFort, E.C., "Pattern Synthesis Based on Adaptive Array Theory," *IEEE Trans. Antennas Propag.* **37**(8), 1011–1018 (August 1989).

Elliott, R.S., and G.J. Stern, "A New Technique for Shaped Beam Synthesis of Equispaced Arrays," *IEEE Trans. Antennas Propag.* **AP-32**(10), 1129–1133 (October 1984).

Evans, R.J., and T.E. Fortmann, "Design of Optimal Line-Source Antennas," *IEEE Trans. Antennas Propag.* **AP-23**(3), 342–347 (May 1975).

Guenad, B., S.M. Meriah, and F.T. Bendimerad, "Multibeam Antennas Array Pattern Synthesis Using a Variational Method," *Radioengineering* **16**(2) 28–33 (June 2007).

Law, D.C., S.A. McLaughlin, M.J. Post, B.L. Weber, D.C. Welsh, and D.E. Wolfe, "An Electronically Stabilized Phased Array System for Shipborne Atmospheric Wind Profiling," *Journal of Atmospheric and Ocean Technology* **19**(6), 924–933 (June 2002).

Levine, D., "Maximum Antenna Gain of Shaped Beams," Technical Report AFTR-6505, Wright-Patterson AF Base, Ohio, March, 1951.

Lewis, G.M., "Radiating Element Design for a Multi-Octave Phased Array Aperture," 5th EMRS DTC Technical Conference, Edinburgh, 2008; available at http://emrsdtc.com/conferences/2008/downloads/conference_papers/A3.pdf.

Liang, C.-H., L. Li, and X.-J. Dang, "Inequality Condition for Grating Lobes of Planar Phased Array," *Progress In Electromagnetics Research B* **4**, 101–113 (2008).

Mahanti, G.K., A. Chakrabarty, and S. Das, "Phase-Only and Amplitude-Phase Synthesis of Dual-Pattern Linear Antenna Arrays Using Floating-Point Genetic Algorithms," *Progress in Electromagnetics Research, PIER* **68**, 247–259 (2007).

Mahanti, G.K., S. Das, and A. Chakraborty, "Design of Phase-Differentiated Reconfigurable Array Antennas with Minimum Dynamic Range Ratio," *IEEE Antennas Wireless Propag. Lett.* **5**, 262–264 (2006).

Mailloux, R.J., *Phased Array Antenna Handbook*, 2nd ed., Ch. 1, "Phased Arrays in Radar and Communication Systems" (Artech House, Boston, 2005).

Olin, I.D., and G.V. Trunk, "Phase Only Aperture Control," Tri-Service Radar Symposium, 2001.

Shavit, R., and S. Levy, "A New Approach to the Orchard–Elliott Pattern Synthesis Algorithm Using LMS and Pseudoinverse Techniques," *Microwave and Optical Technology Letters* **30**(1), 12–15 (July 2001).

Tonn, D.A., and R. Bansal, "Reduction of Sidelobe Levels in Interrupted Phased Array Antennas by Means of a Genetic Algorithm," *International Journal of RF and Microwave Computer-Aided Engineering* **17**(2), 134–141 (March 2007).

Torrealba, R., D.H. Covarrubias, and M. Panduro, "Analysis of Robustness for Convex Optimization Applied to Array Antenna Pattern Synthesis," *Journal of Computer Science* **4**(12), 1036–1041 (2008).

Trastoy, A., and F. Ares, "Phase-Only Synthesis of Continuous Linear Aperture Distribution Patterns with Asymmetric Side Lobes," *Electronics Letters* **34**(20), 1916–1917 (October 1998).

Trastoy, A., and F. Ares, "Phase-Only Control of Antenna Sum Patterns," *Progress in Electromagnetics Research, PIER* **30**, 47–57 (2001).

Vaskelainen, L.I., "Phase Synthesis of Conformal Array Antennas*," IEEE Trans. Antennas Propag.* **48**(6), 987–991 (June 2000).

Voges, R.C., and J.K. Butler, "Phase Optimization of Antenna Array Gain with Constrained Amplitude Excitation," *IEEE Trans. Antennas Propag.* **AP-20**(4), 432–436 (July 1972).

Von Aulock, W.H., "Properties of Phased Arrays," *Proc IRE*, October 1960, pp. 1715–1727.

This page
intentionally
left blank

Appendix A

OPTIMIZED WEIGHTS AND PHASES

The Chebyschev weights and phases optimized for cited flat-top pattern widths described in the report section on "Representative Results" are detailed in Table A1 and Table A2. These are for 50-element linear arrays. Each of the six weight sets of ten Chebyschev polynomial weights defined the 25 independent array phase weights for 50-element linear arrays that were then further optimized. The one set of phases without the source Chebyschev weight set is for a 50-element linear array of $\lambda/\sqrt{3}$ spaced elements used for the rectangular profile pattern shown in Fig. 33. Like all results from optimization procedures, these values cannot be verified to be "globally optimum"; however, the results using the basic array structure equations fulfilled the array pattern specifications, as acceptable. Tables A3 and A4 relate to weights and phases for a 200-element linear array of elements spaced $\lambda/2$ apart.

Table A1 — Optimized Chebyschev Weights for a Linear Array of 50 Elements Spaced $\lambda/2$ Apart

	±5°	±10°	±20°	±30°	±40°	±50°
W_2	3.03183	4.15328	16.52190	11.13650	15.02533	16.09508
W_4	−0.34280	0.48531	2.71907	0.79457	1.05451	1.40637
W_6	−0.25127	0.50599	0.37137	0.67058	0.95711	0.78676
W_8	0.12125	0.80705	1.31209	0.90702	0.80954	0.78898
W_{10}	−0.04840	0.37223	1.25486	0.95151	0.73612	0.75018
W_{12}	0.04558	0.60845	0.34321	0.71754	0.64657	0.53617
W_{14}	−0.02459	0.54914	−0.89402	0.06230	0.29734	0.18835
W_{16}	−0.01851	0.80964	−0.04263	0.47155	−0.02809	−0.23551
W_{18}	−0.01806	0.24622	0.21245	0.00355	0.15825	0.46523
W_{20}	0.00500	0.20249	0.26844	−0.08284	−0.11005	−0.01485

Table A2 — Further Optimization of Element Radian Phases from Those Using the Weights in Table A1

	±5°, λ/2	±10°, λ/2	±10°, λ/√3	±20°, λ/2	±30°, λ/2	±40°, λ/2	±50°, λ/2
δ_1	1.75894	2.45661	−5.35392	−0.13036	3.110529	0.295202	1.504236
δ_2	−0.03526	1.96483	−1.91285	1.17403	0.983487	−1.77344	−0.35928
δ_3	−2.73606	2.82983	−3.97537	1.85285	−0.2446	2.460292	−2.76351
δ_4	1.42541	1.60430	−2.0012	2.71354	−1.30714	0.60362	1.376001
δ_5	0.70362	0.63931	−1.67667	−3.00815	−2.34787	−1.55022	−0.27107
δ_6	0.29308	0.47104	−1.89887	−2.10321	2.583561	2.810866	−1.76132
δ_7	0.19792	0.52108	−0.89628	−1.60981	1.555644	1.478017	2.753894
δ_8	−0.68591	0.37465	−0.62598	−0.82905	0.06707	−0.1481	−0.47459
δ_9	−0.77529	−0.03001	−0.17091	0.03040	−1.55586	−2.11324	−2.83548
δ_{10}	−1.09184	−0.60081	0.138777	0.97294	−3.04415	2.614836	1.11037
δ_{11}	−1.14164	−1.22505	0.087195	1.89394	1.90852	1.577126	0.240071
δ_{12}	−1.32302	−1.79956	0.410125	2.58715	1.054808	0.212817	−0.80698
δ_{13}	−1.35031	−2.24336	1.34662	2.54755	0.406455	−0.78468	−1.30891
δ_{14}	−1.44593	−2.52765	2.524568	−2.31091	0.612065	−1.40042	−2.88035
δ_{15}	−1.56345	−2.69743	2.876612	1.80480	−0.58316	−2.62649	2.024124
δ_{16}	−1.79180	−2.85221	2.912761	−2.73313	−0.77987	1.997893	0.443118
δ_{17}	−1.87218	−3.08731	2.775308	2.79711	−2.05492	1.121805	−1.33611
δ_{18}	−1.94617	2.85271	3.097377	−2.74453	−2.38656	0.495214	−0.00779
δ_{19}	−1.95523	2.46798	4.002032	−2.03553	3.141593	0.064955	−1.95179
δ_{20}	−2.48889	2.17319	4.47216	−1.77273	1.873828	−0.32198	−0.28513
δ_{21}	−2.95497	2.09414	4.361704	−0.53219	2.155837	−1.22725	−1.64146
δ_{22}	−3.03519	2.27750	4.128928	−2.69325	1.908178	−1.11184	−1.7038
δ_{23}	−3.11892	2.65531	3.666619	−1.23949	2.056258	−1.69202	2.655202
δ_{24}	−3.02355	3.06759	3.478114	−0.94091	1.802566	−1.83539	−3.08601
δ_{25}	−3.20867	−2.95018	3.611831	−0.92814	2.846404	−2.37612	−3.07736

Table A3 — Optimized Chebyschev Polynomial Weights for a Linear Array of 200 Elements Spaced λ/2 Apart

W_2	W_4	W_6	W_8	W_{10}	W_{12}	W_{14}	W_{16}	W_{18}	W_{20}
6.26124	−0.72345	−0.16951	0.62585	0.99692	0.79339	1.35673	1.05067	0.67826	0.64469

Table A4 — Optimized Radian Phases for the Same 200-Element Array Used for Table A3

δ_1	11.16711	δ_{26}	1.865863	δ_{51}	−3.44613	δ_{76}	−5.33906
δ_2	2.84354	δ_{27}	1.604648	δ_{52}	−3.69609	δ_{77}	−5.45635
δ_3	0.768589	δ_{28}	1.354173	δ_{53}	−3.94227	δ_{78}	−5.57484
δ_4	1.065749	δ_{29}	1.136642	δ_{54}	−4.14872	δ_{79}	−5.6792
δ_5	2.13032	δ_{30}	0.944992	δ_{55}	−4.29219	δ_{80}	−5.76697
δ_6	3.786219	δ_{31}	0.763292	δ_{56}	−4.37799	δ_{81}	−5.84564
δ_7	5.338698	δ_{32}	0.583714	δ_{57}	−4.43427	δ_{82}	−5.92056
δ_8	6.3447	δ_{33}	0.400327	δ_{58}	−4.51031	δ_{83}	−5.99399
δ_9	6.614527	δ_{34}	0.205545	δ_{59}	−4.63646	δ_{84}	−6.07042
δ_{10}	6.165517	δ_{35}	−0.00763	δ_{60}	−4.84826	δ_{85}	−6.16338
δ_{11}	5.325213	δ_{36}	−0.23176	δ_{61}	−5.11769	δ_{86}	−6.31823
δ_{12}	4.648897	δ_{37}	−0.44287	δ_{62}	−5.35626	δ_{87}	−6.59043
δ_{13}	4.235666	δ_{38}	−0.62135	δ_{63}	−5.38781	δ_{88}	−6.94848
δ_{14}	4.033099	δ_{39}	−0.78337	δ_{64}	−5.09268	δ_{89}	−7.26011
δ_{15}	3.960763	δ_{40}	−0.96071	δ_{65}	−4.52695	δ_{90}	−7.41443
δ_{16}	3.882654	δ_{41}	−1.1871	δ_{66}	−3.98989	δ_{91}	−7.415
δ_{17}	3.683036	δ_{42}	−1.44949	δ_{67}	−3.82633	δ_{92}	−7.30211
δ_{18}	3.360766	δ_{43}	−1.7421	δ_{68}	−4.22115	δ_{93}	−7.15102
δ_{19}	3.386698	δ_{44}	−2.07549	δ_{69}	−4.93342	δ_{94}	−7.02049
δ_{20}	2.763489	δ_{45}	−2.31971	δ_{70}	−5.52442	δ_{95}	−6.94335
δ_{21}	2.600962	δ_{46}	−2.53792	δ_{71}	−5.75941	δ_{96}	−6.89895
δ_{22}	2.491291	δ_{47}	−2.70152	δ_{72}	−5.67392	δ_{97}	−6.84309
δ_{23}	2.391478	δ_{48}	−2.84222	δ_{73}	−5.44795	δ_{98}	−6.75383
δ_{24}	2.268009	δ_{49}	−3.00597	δ_{74}	−5.28841	δ_{99}	−6.63973
δ_{25}	2.096114	δ_{50}	−3.21223	δ_{75}	−5.26368	δ_{100}	−6.53462

This page
intentionally
left blank

Appendix B

LINEAR ARRAY ELEMENT PHASE OPTIMIZER

VISUAL BASIC MACRO OPERATING CONCEPT

The following Visual Basic (VB) macro was used for optimizing the phases of the linear array of elements described in this report. Although a spreadsheet is not shown, sufficient non-executable comments are included within the program on row, column, and cell contents and locations, that the complete spreadsheet can be designed and the macro used directly. Although this macro is based on optimizing an initial list of phases, straightforward modification would enable instead the optimization of Chebyschev weights, as long as the optimization criteria use the corresponding phases, as noted in the report sections on "Optimization" and "Optimization Convergence."

```
Sub Phaseoptimizer()
'
' Phaseoptimizer Macro
' Iterative repetitions of Solver using phase list columns: red, green, blue
' Red column (F11:F35), Current operating phase list
' Blue column (H11:H35), Best list during iterations
' Green column (G11:G35), Random update of Blue copied to red
' Random control: H11+$G$9*(RAND()-0.5)
' Phase change limits: Cells(9,4)=+2*pi(); Cells(10,4)=-2*pi()
' Current flat-top ripple: Cells(I8)
' Flat-top ripple constraint: Cells(9,9)

For I = 1 To 50
' Number of times Solver is repeated
'
Cells(5, 2) = I
'
' Cells(2,9) current maximum sidelobe
' Cells(2,14) prior better sidelobe

If Cells(2, 9) < Cells(2, 14) Then
'
' A new better and lower maximum sidelobe has been found
' Copy the new value into N2, then the red column into blue
' Then green column into red and optimize again

Cells(2, 9).Select
Selection.Copy
Cells(2, 14).Select
```

```
Selection.PasteSpecial Paste:=xlPasteValues, Operation:=xlNone, SkipBlanks _
    :=False, Transpose:=False
Range("F11:F35").Select
Selection.Copy
Range("H11").Select
Selection.PasteSpecial Paste:=xlPasteValues, Operation:=xlNone, SkipBlanks _
    :=False, Transpose:=False

Range("G11:G35").Select
Application.CutCopyMode = False
Selection.Copy
Range("F11").Select
Selection.PasteSpecial Paste:=xlPasteValues, Operation:=xlNone, SkipBlanks _
    :=False, Transpose:=False
'
' Current maximum sidelobe during optimization in $I$2
'
SolverOk SetCell:="$I$2", MaxMinVal:=2, ValueOf:="0", ByChange:="$F$11:$F$35"
SolverAdd CellRef:=Range("F11:F35"), Relation:=1, FormulaText:=Cells(9, 4)
SolverAdd CellRef:=Range("F11:F35"), Relation:=3, FormulaText:=Cells(10, 4)
SolverAdd CellRef:=Range("$I$8"), Relation:=3, FormulaText:=Cells(9, 9)
SolverSolve UserFinish:=True
SolverFinish KeepFinal:=1

Else

' The current optimized sidelobe level in cell I2 is poorer than the best saved in N2
' Just copy the green column to the red column and optimize again

Range("G11:G35").Select
Selection.Copy
Range("F11").Select
Selection.PasteSpecial Paste:=xlPasteValues, Operation:=xlNone, SkipBlanks _
    :=False, Transpose:=False
SolverOk SetCell:="$I$2", MaxMinVal:=2, ValueOf:="0", ByChange:="$F$11:$F$35"
SolverAdd CellRef:=Range("F11:F35"), Relation:=1, FormulaText:=Cells(9, 4)
SolverAdd CellRef:=Range("F11:F35"), Relation:=3, FormulaText:=Cells(10, 4)
SolverAdd CellRef:=Range("$I$8"), Relation:=3, FormulaText:=Cells(9, 9)
SolverSolve UserFinish:=True
SolverFinish KeepFinal:=1


End If
Next I

End Sub
```

3D PATTERN CALCULATION

This Excel macro enables pattern calculation using the pattern shape phases that are first copied into cells in one of two spreadsheets "Angcalc." Another spreadsheet, "Results," lists a column of elevation values used in the calculation and a row of azimuth values used in the calculation. The macro first scans pairwise entries of each azimuth and elevation, and copies them to "Angcalc." Calculation using Excel's complex functions is fast and provides pattern field amplitude, termed "Sumvolts," that is then copied into the corresponding azimuth, elevation cell in "Results." The macro is started from the "Results" spreadsheet and cycles with the "Angcalc" until all the elevation-azimuth combinations are completed. This provides the complete field amplitude pattern from which the decibel values can be calculated and applied to the pattern plotting program. In the work described here, a current version of SigmaPlot was used.

```
Sub macro3D()
'
' macro3D Macro
' A total volume within plus/minus 30 degrees, Az and El in 0.5 degree steps is spanned
‘ Elevation angles are in cells (C5:C125)
‘ Azimuth values Are in cells (D4:DT4)
‘ Other intervals can be specified, as required
' Macro is started from the worksheet "Results"
' Macro first selects phi (elevation), then cycles through all theta (azimuth) values.
' Then a new phi value is selected and the azimuth cycle repeated
' Successively calculated sumvolts results are entered into the Results spreadsheet
'
Dim J As Integer
Dim I As Integer
' J equals phi values
' I equals theta values

For J = 5 To 125
   Cells(J, 3).Select
   Selection.Copy
   Sheets("Angcalc").Select
   Range("B6").Select
   ActiveSheet.Paste
' Phi value selected and entered in Angcalc, cell B6

For I = 4 To 124
   Sheets("Results").Select
   Cells(4, I).Select
   Application.CutCopyMode = False
   Selection.Copy
   Sheets("Angcalc").Select
   Range("B7").Select
   Selection.PasteSpecial Paste:=xlPasteValues, Operation:=xlNone, SkipBlanks _
      :=False, Transpose:=False
' Theta value selected and entered in Angcalc, cell B7
```

```
Range("C11").Select
Application.CutCopyMode = False
Selection.Copy
Sheets("results").Select
Cells(J, I).Select
Selection.PasteSpecial Paste:=xlPasteValues, Operation:=xlNone, SkipBlanks _
    :=False, Transpose:=False
' Sumvolts value in C11 in "Angcalc" copied into corresponding
' azimuth/elevation cell in worksheet "results"

Next I
' Select another theta azimuth and repeat until the -30 to +30 theta interval is complete

Next J
' Select another phi elevation and cycle through all theta values

End Sub
```